DRAFT

International Energy Agency Wind Technology Collaboration Programme Task 27 Small Wind Turbine Technical Report

Technical Recommendations for Consideration of Future International Electroctechnical Commission (IEC) 61400-2 Standard

September 2018

TECHNICAL REPORT

INTERNATIONAL ENERGY AGENCY WIND TECHNOLOGY COLLABORATION PROGRAMME TASK 27 SMALL WIND TUBINE TECHNICAL REPORT

Prepared for the
International Energy Agency Wind Implementing Agreement

Edited by:
Trudy Forsyth and Ruth Baranowski
Wind Advisors Team
8460 W. 106th Avenue
Broomfield, Colorado 80021 United States

With contributions from:

- Jonathan Whale, Amir Tabrizi, and Anup KC, Murdoch University, Australia
- Mauro Peppoloni, Kurt Leonhartsberger, University of Applied Sciences Technikum Wien, Austria
- Mark Runacres, Vrije Universiteit Brussels, Belgium
- Charlie Dou, Chinese Wind Energy Association, Jianwen Wang, Liru Zhang, Yali Hou, Wenxin Wang, Inner Mongolia University of Technology, China
- Peggy Friis and Davide Conti, Technical University of Denmark, Denmark
- Raymond Byrne, Dundalk Institute of Technology, Ireland
- Takaaki Kono, Kanazawa University, Hikaru Matsumiya, Hikaru Wind, Japan
- Maciej Karczewski, Piotr Domagalski, Institute of Turbomachinery, Lodz University of Technology, Poland
- Seok-woo Kim, Korea Institute of Energy Research, Republic of Korea
- Ignacio Cruz Cruz, Francisco Toja, Luis Cano, Luis Arribas, CIEMAT, Spain
- Hsu, Chung-Chun, Taiwan Small and Medium Wind Association, Taiwan
- Heidi Tinnesand, National Renewable Energy Laboratory, Neil Kelley, Wind Advisors Team, United States

September 2018

The International Energy Agency (IEA) Wind Technology Collaboration Programme (TCP) functions within a framework created by the IEA. Views, findings and publications of IEA Wind do not necessarily represent the views or policies of the IEA Secretariat or of its individual member countries. IEA Wind is part of IEA's TCP.

DRAFT

PREFACE

This technical report provides a series of recommendations based on Task 27 research results that should be considered in future standards-making activities for IEC 61400-2. While these recommendations are preliminary in nature and require further validation, many of the results suggest changes to turbulence characteristics, loads models and methods, as well as the development of a new turbine design classification. Small wind turbines are failing around rated wind conditions largely due to high shearing stress in weakly stable conditions. Inclusion of the turbulent shearing stress and the Richardson number stability parameters as inputs to load cases and structural requirements will begin to capture the more realistic small wind turbine operating conditions. It is recommended that both modeling and measurements be used to validate small wind turbine design.

IEA Wind TCP Task 27 work started from the linkage of back-to-back meetings of small wind turbine experts who developed both the third revision of the IEC 61400-2 standard "Part 2: Small wind turbines" and the Recommended Practice (RP 12) titled "Consumer Labels for Small Wind Turbines." During the development of IEC standard 61400-2, it became apparent that turbulence design parameters were likely inadequate to capture turbulence seen in turbine owners' sites and to understand potential fatigue impacts on small wind turbine structural designs. Table P-1 shows the IEA Wind Task 27 experts involved in the research behind these technical recommendations.

Table P-1. IEA Wind Task 27 Participants during this Period (2012-2018)

Country	Contracting Party	Active Organizations
Australia	Clean Energy Council	Murdoch University
Austria	Bundesministerium für Verkehr, Innovation und Technologie	University of Applied Sciences Technikum Wien
Belgium	General Policy and International Relations, Directorate General Energy	Vrije Universiteit Brussels
China	Chinese Wind Energy Association	China Wind Energy Association and Inner Mongolia University of Technology, Tiawan Small & Medium Wind Turbine Association, Institute of Nuclear Energy Research
Denmark	Danish Energy Agency	Risø Danish Technology University
Ireland	Sustainable Energy Authority Ireland	Dundalk Institute of Technology
Japan	New Energy and Industrial Technology Development Organization (NEDO)	Kanazawa University, Mie University
Poland		Lodz University of Technology
Republic of Korea	Government of Korea	Korea Institute of Energy Research
Spain	CIEMAT	CIEMAT (co-Operating Agent)
United States	U.S. Department of Energy; National Renewable Energy Laboratory (NREL)	NREL, Wind Advisors Team (co-Operating Agent)

A special acknowledgement goes to Neil Kelley for sharing his insight on turbulence and its effects on wind turbines, educating us on the sensitivities of atmospheric conditions and answering our questions.

Trudy Forsyth, Operating Agent

IEA Wind TCP, Task 27

www.ieawind.org

Ignacio Cruz Cruz, Operating Agent

IEA Wind TCP, Task 27

www.ieawind.org

September 2018

DISCLAIMER:

IEA Wind TCP functions within a framework created by the IEA. The views, findings and publication of this report do not necessarily represent the views or policies of the IEA Secretariat or of all of its individual member countries.

DRAFT

TABLE OF CONTENTS

DRAFT

LIST OF FIGURES

DRAFT

DRAFT

LIST OF TABLES

DRAFT

LIST OF ABBREVIATIONS

CFD	computational fluid dynamics
CTKE	coherent turbulent kinetic energy
DEL	damage equivalent load
EDC	extreme direction change
FBM	flapwise bending moment
IEA	International Energy Agency
IEC	International Electrotechnical Commission
KHI	Kelvin-Helmholtz Instability
NREL	National Renewable Energy Laboratory
NTM	Normal Turbulence Model
NWTC	National Wind Technology Center
TCP	Technology Collaboration Programme
TI	turbulence intensity
TKE	turbulent kinetic energy
VAWT	vertical-axis wind turbine

DRAFT

EXECUTIVE SUMMARY

This technical report resulted from the need to gather new measurements, simulations and models of highly turbulent sites to better understand structural design limitations. In the process of investigating a new Normal Turbulence Model (NTM), the following new ways of describing turbulence have been developed and proposed: a new small wind turbine[1] design classification, a modified equation for the load case Extreme Direction Change for turbulent sites, an expansion of required vibration analyses, and a new simplified model for vertical-axis wind turbines (VAWTs).

While many of these results have been independently validated, they are still preliminary in nature and can only benefit from continued, targeted field test measurements, simulations and models. Recommendations are provided on how to attain those field test measurements.

As a result of the Task 27 work and consultation with Neil Kelley, the understanding of the fatigue sensitivities for small wind turbines has been highlighted, and further study of what happens in weakly stable flow during winds of approximately 10 m/s or rated power are needed.

It is hoped that this report and the subsequent work will provide a deep technical background on all small wind turbine sensitivities to turbulence and intrinsic oscillations with quantifiable results that will guide future standards-making activities for IEC 61400-2. During the most recent third revision, the IEC 61400-2 standards-making team realized that most small wind turbines are sited in areas of high turbulence and the standard only required a reference turbulence intensity value I_{15} of 0.18, likely not typical of most owners' sites. There were no data to inform Task 27 experts on frictional or vertical velocities found relatively near the ground.

We are beginning to understand these vertical velocities and their impacts on the blade flapwise, in-plane and torsional bending moments, fatigue and other load conditions. There is time to continue this key research before the IEC 61400-2 cure date expires in 2021. There have been continued discussions on how to help transition the Task 27 results for standards-making to a new distributed wind task. This report documents the results we have achieved so far and a description of future work that will expand and solidify our current understandings.

This technical report will be useful to new standards-making experts, certification bodies and test laboratories that support small wind turbine certification. It will also be useful to small wind turbine designers, academicians and small wind turbine researchers.

The Task 27 effort has been designed to continue global research toward refining the IEC small wind turbine standard, thereby linking both the past and future versions of IEC standards with IEA research.

[1] Less than 200 m² rotor-swept area

DRAFT

1. BACKGROUND INFORMATION AND OBJECTIVES OF TASK

There were two primary goals for the work performed under IEA Task 27. The first was to conduct global, shared research to better understand technical parameters within IEC 61400-2 that were troubling, and the second was to take these research findings and help transfer the results to a useful, practical guide on micrositing small wind turbines. This document provides recommendations for consideration by the next IEC maintenance team writing the IEC 61400-2 fourth revision.

In 2009, IEC 61400-2 third revision and IEA Task 27 meetings were held back to back. At that time, there was general consensus that a few areas of the 61400-2 standard required research to allow standards-making experts to make recommendations or requirements within the standard.

Anecdotally, we know that a few wind turbine failures have occurred, most likely due to loads generated by highly turbulent wind. While some of these turbines met the requirements of the standard and achieved certification, we know that the standards are not as robust as they should be. This is understandable when one considers the stochastic nature of turbulence. Further validation and continued research are critical to ensuring that certified small wind turbine designs are more robust and durable. Such research is also of importance for certification bodies to aid engineers in conducting more comprehensive certifications.

Task 27 experts were involved in analyzing additional three-dimensional wind resource data, which were initially used to get a preliminary understanding of longitudinal wind direction; i.e., parallel to the main shaft. But then the impact of the vertical inflow became apparent, and new measurements were made in highly turbulent sites such as rooftops. Ultrasonic measurements of wind speed were preferred due to the assumption that 10-Hz to 20-Hz data were required to accurately characterize the turbulence in the wind flow over a complex terrain.

A common approach to collecting and analyzing new three-dimensional data sets was developed and included performing a site calibration and characterizing the wind resource and power production at turbine sites. In general, researchers at each test site performed wind resource measurements at multiple heights and included turbulence information and temperature data to understand the impact of atmospheric stability through the Richardson number. Measurements on rooftops were made in the middle of the roof to reduce impacts from roof edge effects.

Computational fluid dynamics (CFD) models were developed for some of these test sites and for simple shapes mimicking a roof. In general, the CFD simulations conducted to date assume a neutrally stable atmosphere, which reduces the probability of fully understanding the full three-dimensional turbulent structure of the flow in and around buildings. However, the available expert CFD simulation results helped to inform and gave trend information on the very complex flow patterns around buildings and developed confidence in usage of different simulation methods such as Large-Eddy Simulations and Reynolds-Averaged Natvier-Stokes, or RANS, modelling approaches.

There are two companion documents summarizing the 6 years of Task 27 work, and these documents may be useful in understanding the summary for standards recommendations. The first document is a Compendium of Task 27 Case Studies, which includes the details of the work

DRAFT

and referenced papers and journal articles. The second document is a practical Recommended Practice on Micrositing Small Wind Turbines in Highly Turbulent Sites, which has limited technical discussion but emphasizes both qualifying and quantifying an individual site's wind resource.

The recommendations for informing the next round of standards development for IEC 61400-2 are divided into two groups. The first are recommendations for better characterizing turbulence typically seen at small wind turbine sites and an understanding of the critical nature of the typical site turbulence. The second set of recommendations is focused on proposed changes to the structural design section of the IEC standard.

Small wind turbines operate relatively close to the ground as compared with the larger, modern multi-megawatt machines now operating in wind farms onshore and offshore. They can be installed in a wide variety of locations ranging from unobstructed as well as forested flat terrain to within very complex landforms. Because the ultimate operating environment of many small wind turbines is often unknown, the design of these machines must be sufficiently robust to provide an efficient and safe operation for an extended period of time without excessive maintenance. A key factor in meeting these goals is for the turbine design to withstand the exposure to a wide range of turbulent flows seen in actual operating conditions.

2. TECHNICAL RECOMMENDATIONS FOR CHARACTERIZING TURBULENCE

Turbulence in the turbine inflow has a significant influence on the power production and the lifetime of turbine components. The primary source of degraded performance and component reliability is the unsteady aerodynamic effects created by turbulent flow over the turbine rotor blades. The unsteady aerodynamic affects the ability of the blades to efficiently generate lift, regardless of the rotor orientation, and creates dynamic loads on the rotor blades that in turn excite a range of vibrational frequencies associated with the turbine structure that must be dissipated by the turbine structure.

Published power curves are rarely representative for the performance of small wind turbines in highly turbulent conditions. This is because wind turbine power curves are typically developed based on measurements taken at sites with relatively low turbulence intensity compared to many small wind turbine sites with high turbulence, such as rooftops, urban areas or places with high surface roughness from the surrounding landscape.

The NTM of the IEC 61400-2 standard significantly underestimates the turbulence levels or intensity for highly turbulent conditions in which many small wind turbines operate, such as in an urban or peri-urban terrain. Short of avoiding turbulent sites altogether, particular care should be taken in assessing the turbulence on the site, for all relevant wind directions, when considering a small wind project.

Assessment of turbulence for a highly turbulent site should at least entail the usage of a model that:

DRAFT

- Has a representative V_{wind}- σ slope parameter
- Has a representative average wind speed velocity
- Has a representative reference turbulence intensity at the representative average wind speed
- Can introduce a representative integral length scale parameter.

2.1 Normal Turbulence Model for Highly Turbulent Sites

The standard wind class definitions described in the IEC 61400-2 standard, with a turbulence intensity value of I_{15}=0.18 are not suitable for many installations in highly turbulent sites. Such sites are often urban or peri-urban areas, where site-specific characteristics such as a number of buildings/trees/hills, their heights and lengths relative to turbine rotor and tower size, atmospheric conditions such as frequently varying wind direction, wind speed and air temperature are of the paramount importance for turbine micro-siting. These characteristics must be considered because of the complex inflow caused by the flow separations and reattachments as the wind passes over and around obstacles and terrain changes. Table 1 shows the current IEC 61400-2 standard's definitions of SWT wind classes.

Table 1. IEC 61400-2 Small Wind Turbine Design Classes

SWT Class		I	II	III	IV	S
V_{ref}	(m/s)	50	42,5	37,5	30	Values to be
V_{ave}	(m/s)	10	8,5	7,5	6	specified
I_{15}	(-)	0,18	0,18	0,18	0,18	by the
a	(-)	2	2	2	2	designer

where

- the values apply at hub height, and
- I_{15} is the dimensionless characteristic value of the turbulence intensity at 15 m/s,
- a is the dimensionless slope parameter to be used in equation (7).

All of the classes, despite having different 50-year maximum 10-minute averaged reference wind speed V_{ref} and different average wind speeds V_{ave}, are identically defined in terms of reference turbulence intensity (I_{15} = 0.18) and the slope parameter (a = 2). Essentially, this would create an identical 90th percentile curve of representative measure of turbulence intensity for which a small wind turbine of class I/II/III/IV would have to be designed. The normal turbulence of the standard is expressed as

$$\sigma_{U,90\%} = \frac{I_{15}(15 + aU)}{a + 1} = \frac{0.18(15 + 2U)}{3} \quad (1)$$

Meanwhile, years of exploitation of small wind turbines show that they do not react well to highly turbulent conditions. Figure 1 shows an example of 90th percentile distributions of turbulence intensities measured at an urban site in Australia and a rural site in Sweden. Both characteristics are compared to the existing definition of reference turbulence intensity (TI) curve, as based on IEC classes and Equation 1 above.

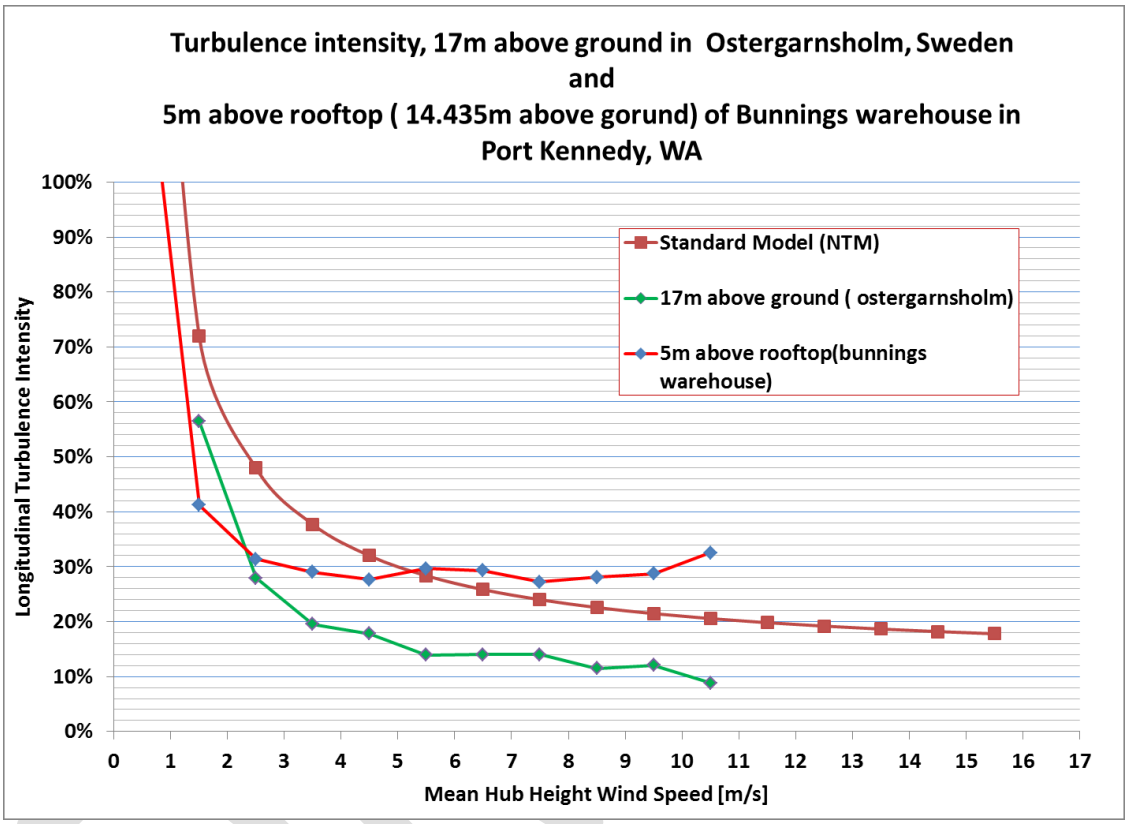

Figure 1. 90th percentile distributions of turbulence intensity in function of wind speed for an urban site in Port Kennedy, Australia (atop Bunnings Warehouse) and for a rural site in Osterharnsholm, Sweden

It is evident that while a rural site adheres to the current definition, the plot for the urban site is settling at higher turbulence intensity than the IEC reference curve proposes. For example, at 10 m/s the IEC standard imposes reference TI of about 20%. The rural site measurement is 10%, but the urban site data shows a 30% TI.

Figure 2 shows mean and 90th percentile distributions for an urban site in Japan and confirms the above findings. For this site, even the mean TI distribution runs over the reference TI curve from 6 m/s on and settles at about 30% TI. At the same time, the 90th percentile of TI at 10 m/s is estimated at 33% for this site. A small band that separates the 90th percentile distribution from the mean suggests that nearly all data points measured at this site are likely to be well above the IEC curve. Usage of the IEC standard NTM for this site would result in a significant under-

representation of the turbulent field.

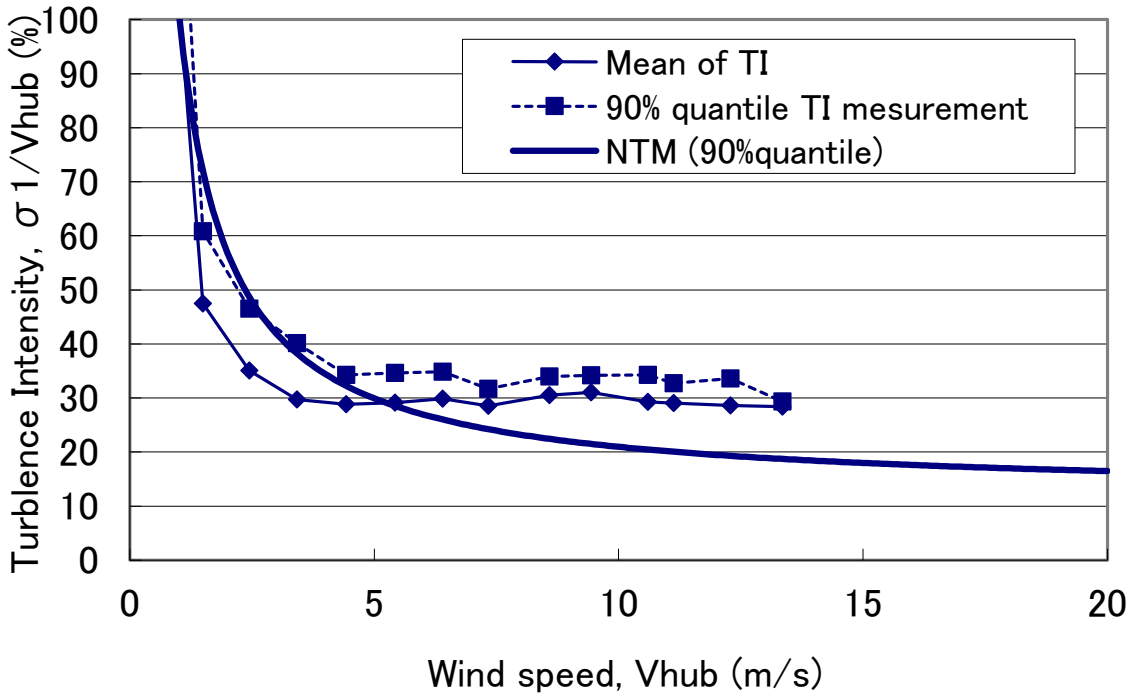

Figure 2. Mean and 90th percentile distributions of turbulence intensity in function of wind speed for an urban site in Japan

We have data for another site, a 95-m-tall building located in a city center in a major European capital (Figure 3). The measurements were taken for a full year in 2013 to investigate the site as a possible small wind turbine location. As before, the graph shows a red curve that is derived based on current IEC recommendations. The distribution of 90th percentile points for this site is approaching 40% at 10 m/s. This is by far the highest value and much above the reference TI suggested by the IEC. This potentially could lead to a situation in which a small wind turbine designed in accordance with either of the classes (I/II/III/IV) and sited there would not be prepared to withstand loads due to highly turbulent wind speeds at this site. In reality, a much higher turbulent inflow would lead to an increased fatigue of blades and tower.

For example, with a 90% confidence level, the standard recommends using a TI of 0.3 at 5 m/s hub-height speed, where all of the measured data confirms that TI is actually higher. Additionally, as mentioned, little measurement data exist beyond 12 m/s. Consequently, using a reference wind speed of 15 m/s, as currently defined in the standard, is usually not practical. A lower reference speed, for which more data are available, would make more sense.

In Figure 2, a new dashed line curve, fitted to the 90th percentiles, is derived instead to suggest what might be a representative TI distribution for this site. A fit to that curve in the U-σ domain is given in Equation (2). The new reference velocity of 5 m/s with the corresponding reference

turbulence intensity of 45% are more suitable, while the slope parameter is the same (a = 2) as in the current version of small wind turbine wind class definitions.

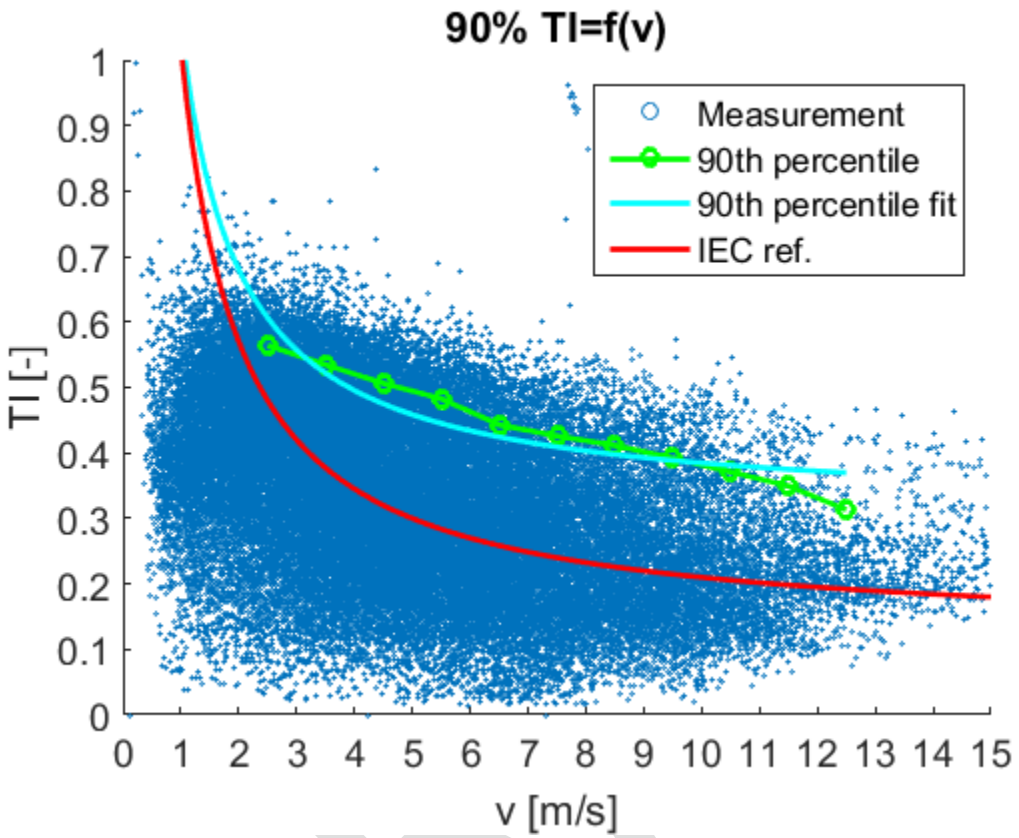

Figure 3. A 10-min averaged measurement data along with 90th percentile points of turbulence intensity in function of wind speed for an urban site (The Hotel, a 95 m tall building) in Brussels, Belgium, measurement period: 02/2013-02/2014

$$\sigma *_{U,90\%} = \frac{I_5(5 + aU)}{a + 1} = \frac{0.45(5 + 2U)}{3} \qquad (2)$$

To explore the impact of Equation (2), another urban site is analyzed in Figure 4. The conservative approach to define the reference TI curve proposed in the example above does not work well for this next site: an urban setting at Nasu Denki, Japan. When the IEC curve with reference I_5 = 0.45 (green) is overlaid on the measured data, it is evident that the measured data do not exhibit such drastic properties at this site. This curve would not be representative for the given site and could be considered too conservative. A small wind turbine design based on such definition would likely produce bulkier blades, thus penalizing turbine performance. For this site, perhaps a more robust approximation can be achieved with a current definition given in the IEC standard (red curve).

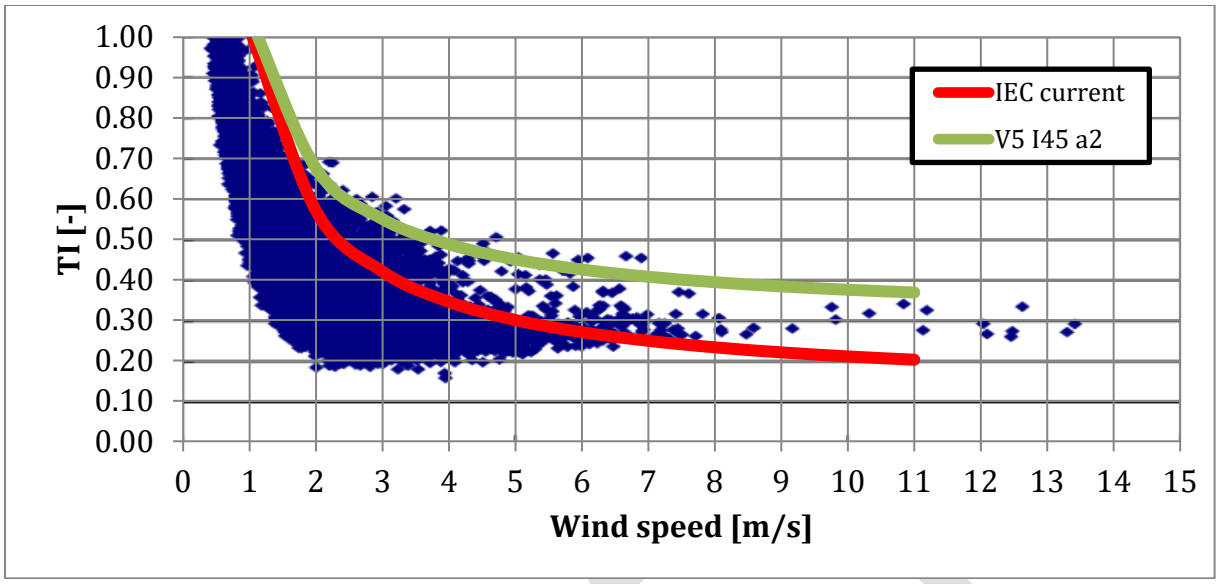

Figure 4. Plot of a turbulence intensity of a longitudinal wind velocity component for an urban site in Nasu Denki, Japan

Therefore, as part of Task 27, the group set out to derive a new NTM. For this reason, measurement campaigns in three urban areas in the Brussels city center were combined: a mast on a Port of Brussels bridge at 10 m agl, a mast atop the 95-m-tall building called The Hotel, and a mast on a 32-m-tall university building called ULB. Figures 5 and 6 present the view of standard deviation and TI in function of wind speed for the combined data set for all three locations.

The measurements were recorded by Thies First Class anemometers between 06/2013-02/2014 for Port of Brussels, 02/2013-02/2014 for The Hotel, 04/2013-02/2014 for the ULB each time by means of two devices mounted at the same height to cancel the mast aerodynamic shadowing effect. The set is by no means exhaustive, but it represents a good portion of city winds averaging from 3.7 m/s for the Port of Brussels, 4.3 m/s for the ULB and up to 5.8 m/s for The Hotel, all at varying heights stretching from fairly close to the street level to more than 100 m agl. The data points are 10-minute averages of longitudinal wind speed component sampled at 1 Hz. For clarity, the 90th percentile distribution is plotted. For the very low speeds <1.5 m/s, the measurement uncertainty becomes a factor due to limitation of the device class and its measurement range; thus this region has been excluded from statistical derivations presented below. For the sake of maintaining a low measurement uncertainty, the velocity interval above >12.5 m/s is not considered either due to the small amount of data in these bins (below 200 records). This is visible in the plot presented in Figure 7. Nevertheless, the variety of sites produces a rich data set for analyses.

DRAFT

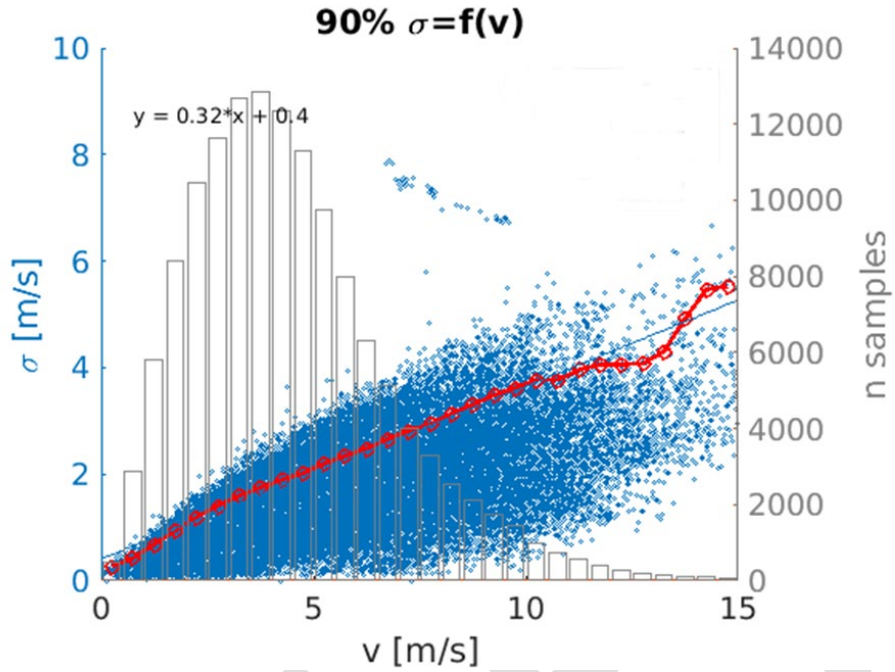

Figure 5. A combined plot of standard deviation in function of wind speed for three urban sites in Brussels, Belgium (The Hotel, ULB and Port of Brussels) showing the standard deviation and its 90th percentile fit. The velocity data histogram is shown as a bar chart

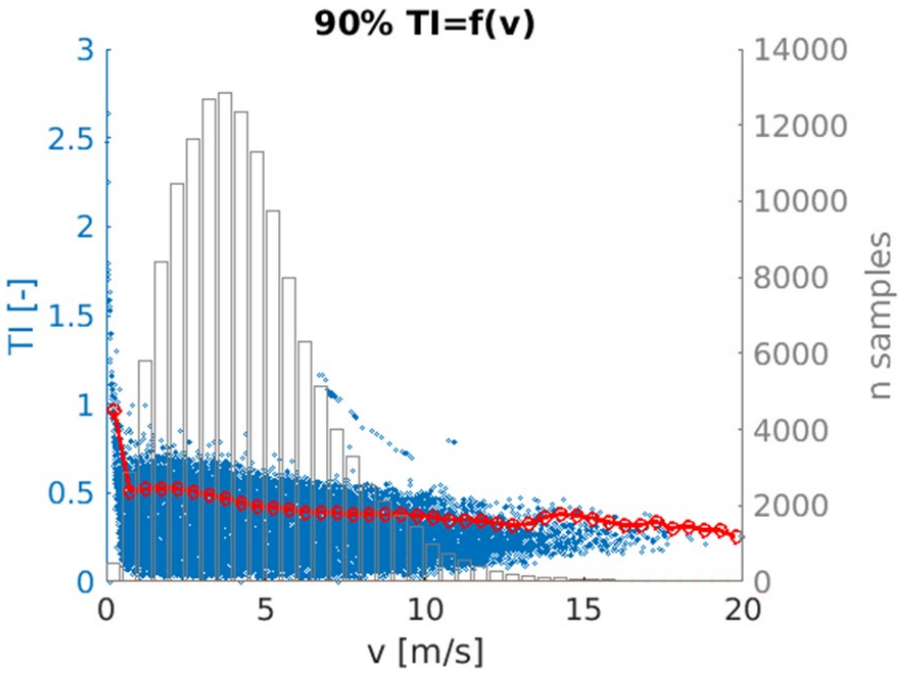

Figure 6. A combined plot of TI in function of wind speed for three urban sites in Brussels, Belgium (The Hotel, ULB and Port of Brussels) showing TI and its 90th percentile fit. The velocity data histogram is shown as a bar chart

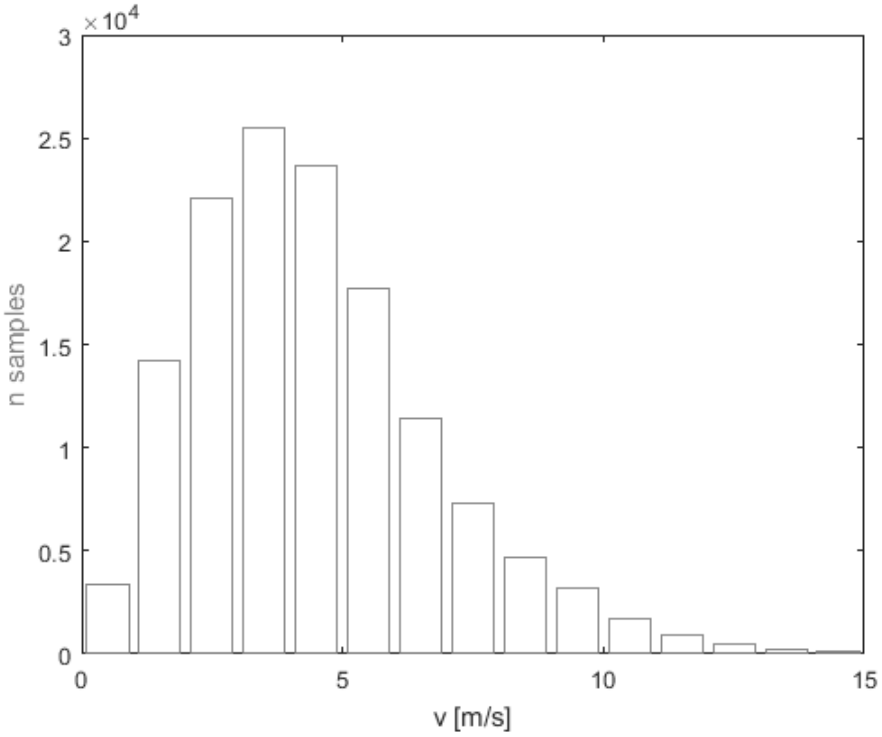

Figure 7. Histogram presenting a combined number of samples per each wind speed bin for all three Brussels sites

The U-σ plot (Figure 5) shows a high degree of linearity up to 10 m/s; however the 90th percentile distribution line begins to change slope beyond this point. This is connected to a convergence of the TI to a constant value at very high velocities. The phenomenon is better visible in the U-TI plot (Figure 6), where for high wind speeds the scatter of data points is smaller and converges onto about 30% in the form of a much narrower band as the speed increases. However, a U-TI equation would not be representative of a lower velocity range, where it is evident that longitudinal turbulence scales linearly with the increasing speed. With this assumption, it would be advisable to derive an equation that is a piece-wise function, having two different equations and a common point, a velocity value at which the mathematical description of turbulent quantities would be based on confidence levels: higher in the U-σ domain for lower wind speeds and higher in the U-TI domain for higher wind speeds.

To derive an approximate value of wind speed beyond which the new NTM should be based on statistical information from the TI-U domain, we propose to compute the variance of σ and of TI for all bins. By normalizing the results via the average variance for all the speed bins, one obtains the plot shown in Figure 8. The velocity value of 6.5 m/s is where the variance of TI begins to be smaller than the variance of σ. This value can be thus proposed as the upper limit of the first piece-wise interval ($0 < U < 6.5$ m/s) and the lower limit for the second piece-wise range ($6.5 < U < 15$ m/s).

DRAFT

In the next steps, the linear equation for the σ-U relationship is derived based on the linear fit ($\sigma=kU+m$) to the data of a desired percentile in the interval up to 6.5 m/s. Beyond this wind speed, the NTM should be based on the hyperbolic fit to a distribution point of desired percentile in the TI-U domain ($TI = \frac{\sigma}{U} = \frac{m}{U} + k$).

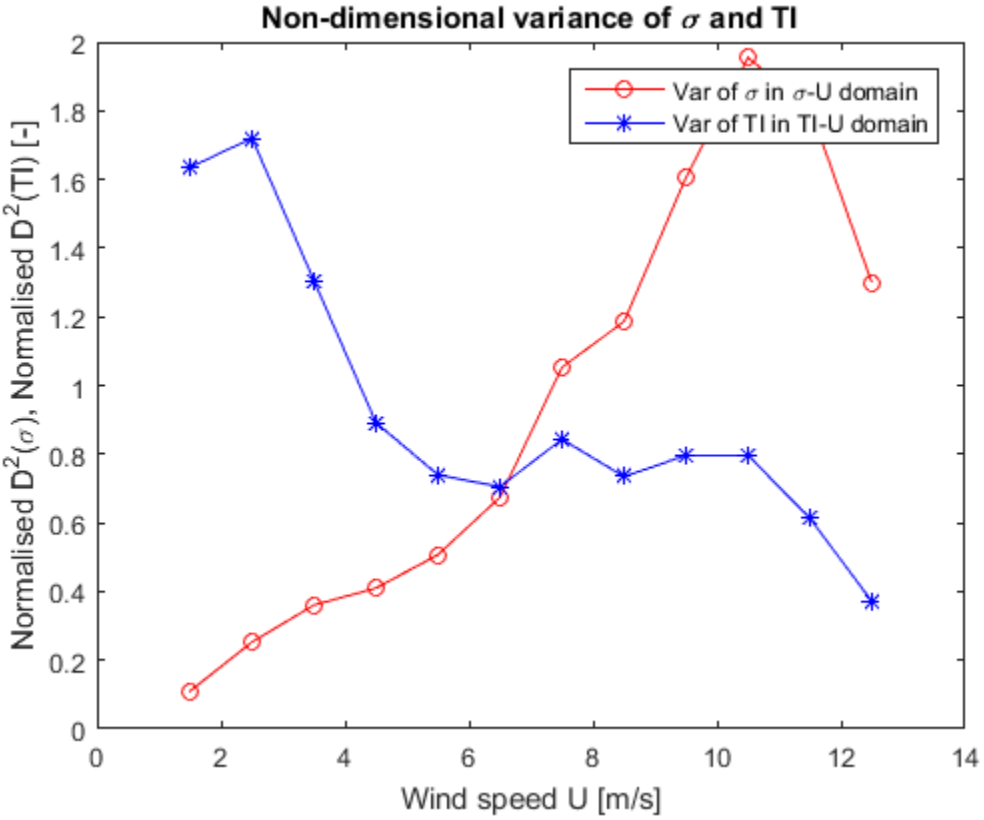

Figure 8. Normalised variance of standard deviation σ and normalised variance of turbulence intensity TI per wind speed bin for measurements at all three urban sites in Brussels

Figure 9 illustrates this concept, presenting two linear equations, each for the respective part of the new NTM. The green equation is a linear fit to the 90th percentile data points for all three Brussels sites presented in Figure 5. The blue equation is a re-worked version of a hyperbolic fit to the 90th percentile data points for all three Brussels sites presented in Figure 6. The hyperbolic equation in the TI-U domain becomes a linear one in the σ-U domain. As the two intervals are approximated separately, the derived piece-wise function is at first discontinuous at the dividing wind speed (hence the intercept of the second equation must be adjusted to make the lines coincident). Although it appears that the new NTM could be entirely replaced by a single linear equation, this is largely due to the scarcity of data at higher wind velocities. For the reasons already mentioned, the σ-U relationship would tend to a constant value if more measurements would be available at wind speeds above 12.5 m/s. This would be manifested by a smaller curve slope and higher intercept for this portion of the model. As a reference, the current definition of the IEC standard is shown in red.

Equation (3) is the proposal for the new NTM in the piece-wise form. Figure 10 presents the model in the turbulence intensity – wind speed domain (TI-U). It is well visible that with the proposed NTM definition, the turbulence at none of the sites, previously analysed in this chapter, would be underrepresented. Such new reference would help to verify the small wind turbine designs for an increased fatigue loading especially crucial at urban sites. The statistically significant definition of the first piece-wise interval on the σ-U domain requires a definition of a reference standard deviation rather than of a reference intensity, as is currently the case. Also, the reference wind speed should be based on a lower velocity, more representative of sites with high turbulence, and a second one in the high-velocity part of the piecewise approximation. Thus σ_5 at $V_{ave} = 5$ m/s and I_{10} at $V_{ave} = 10$ m/s are proposed.

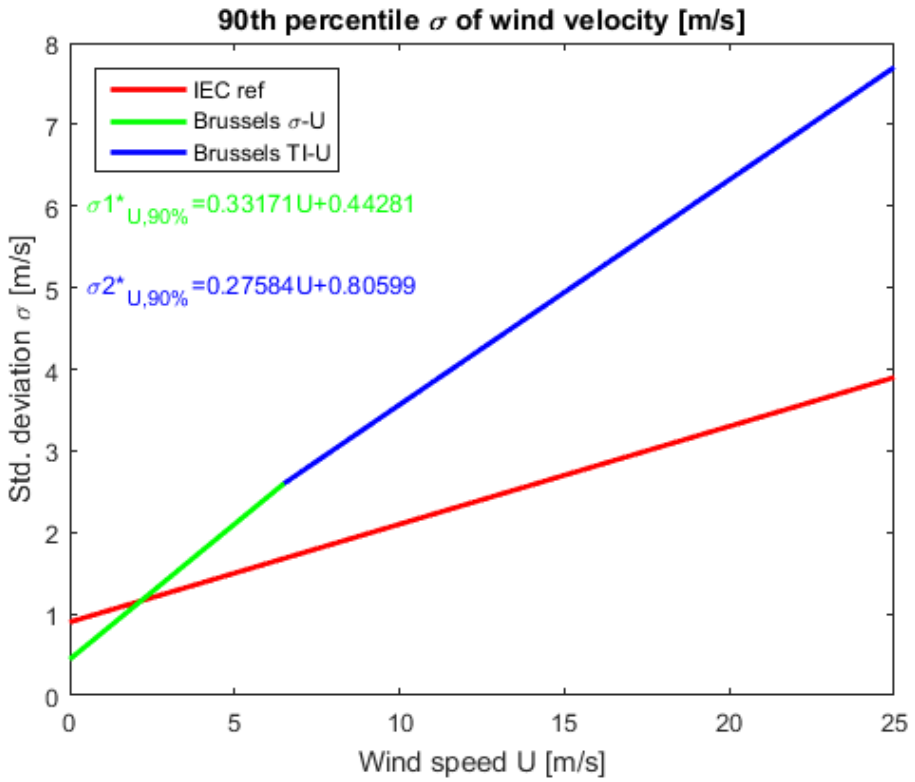

Figure 9. Piece-wise definition of the proposal for the new NTM derived from 90th percentile data fit from measurements recorded for three urban sites in Brussels; the current NTM definition is presented to ease comparison

$$\sigma *^{1,2}{}_{U,90\%} = \begin{cases} \dfrac{I_5(5+aU)}{a+1} = \dfrac{\sigma_5(5+aU)}{5(a+1)} & \text{for } 0 < U < 6.5 \text{ m/s} \\ \dfrac{I_{10}(10+aU)}{a+1} & \text{for } U > 6.5 \text{ m/s} \end{cases} \quad (3)$$

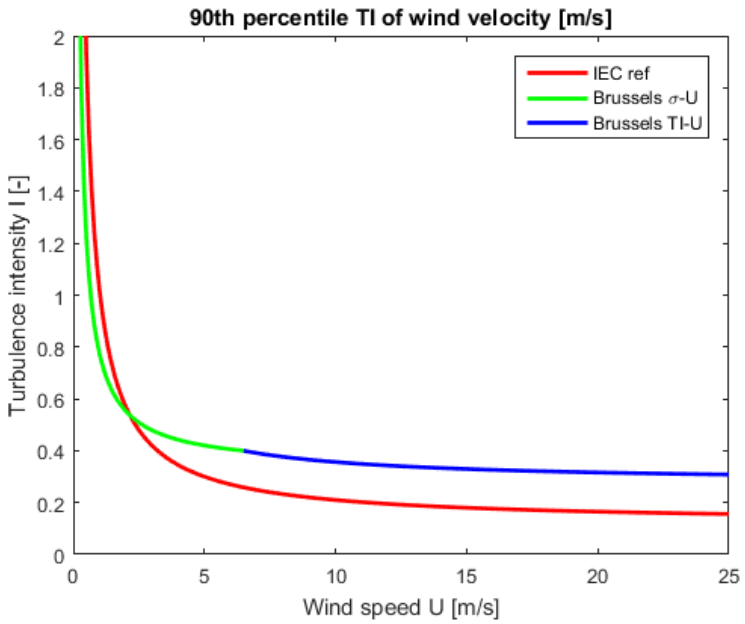

Figure 10. TI-U distribution of piece-wise definition of the proposal for the new NTM derived from 90th percentile data fit from measurements recorded for three urban sites in Brussels; the current NTM definition is presented to ease comparison

Such a definition of the turbulence model requires a change in class definitions; thus we propose a new definition of the urban/highly turbulent small wind turbine class, outlined in Table 2.

Table 2. Basic Parameters for a New Small Wind Turbine Class

SWT Class	Urban/Highly Turbulent
V_{ref} (m/s)	35-40
V_{ave} (m/s) for low-speed regime <10 m/s	5
V_{ave} (m/s) for high-speed regime ≥10 m/s	10
σ_5 (m/s) for low-speed regime <10 m/s	2.1
I_{10} (-) for high-speed regime ≥10 m/s	0.36
a (-)	2

DRAFT

The reference standard deviation and TI values are derived from the presented data set for three sites in Brussels. However, we wish to emphasize that the model needs verification, which will be the focus of the Task 27 group over the next 2 to 3 years. As more data become available, this improved NTM will evolve, and its mathematical expression is likely to change.

2.2 Turbulence

Turbulence is not completely described by indicators such as the TI. In particular, the possible presence of organized, coherent structures in the turbine inflow is not expressed by the value of TI alone. It has been shown (Kelley 2011) that such structures are particularly damaging to small wind turbines.

The presence of coherent structures in the inflow is influenced by the vertical stability of the atmospheric layer in which the turbine rotor resides. When the temperature increases with height, the atmosphere is said to be stable. In that case, a parcel of air that is displaced upward is cooler than its surroundings, has *negative* buoyancy and will sink back to its original position. The opposite occurs when the temperature decreases with height causing the parcel, which is warmer and less dense than its surroundings, to continue to rise due to possessing *positive* buoyancy. Under these conditions, the atmosphere is said to be unstable. Should the temperature of a vertical atmospheric layer remain constant with height (*isothermal*), an air parcel has no net buoyancy and remains at a constant height. This is the definition of *neutral* stability conditions. One of the main attributes of the buoyancy is its influence on the *vertical* component of the wind that is zero in vertical layers that are neutrally stratified. The gradient Richardson number (Ri_g) is a measure of the vertical stability of an atmospheric layer Δz and is expressed as

$$Ri_g = \frac{(g / \overline{\theta}_v)(\overline{\partial \theta_v} / \partial z)}{(\overline{\partial U} / \partial z)^2} \tag{4}$$

where g is the gravitational acceleration, θ_v is the virtual potential temperature (see e.g., Stull 2012, Ch.1), z the height above ground in m and U the wind speed in m/s. The overbar denotes a time average over a suitable period, which for wind turbines has been found to be 10 minutes. (The analysis of wind conditions found over a wide range of wind energy sites has shown that turbulent conditions, as expressed by the standard deviation of U, found quasi-stationarity exists in the turbulent wind field for a record length between 8 and 12 minutes with a median value of 10. Thus a 10-minute measurement period is recommended for the calculation of averages and turbulence spectra and Reynolds stresses.) An unstable atmosphere is shown by $Ri_g < 0$, for a neutral atmosphere $Ri_g = 0$ and for a stable atmosphere $Ri_g > 0$, as follows directly from the definition of the stability classes.

Many three-dimension sonic anemometers provide a temperature output derived from the vertical velocity channel, which is equivalent to the virtual potential temperature and can be used to derive the Richardson number if at least two anemometers are installed at different heights Δz. For this purpose, the gradients present in Equation (4) are replaced by their approximations in the bulk form of the Richardson number, which in case of using linear approximation takes the following form:

$$Ri_B = \frac{g}{\overline{\theta_v}} \frac{\Delta\theta_v}{(\Delta z)^2} \quad (5)$$

While corrections for barometric pressure change and humidity might have a small influence on the absolute value of temperature, that is completely the opposite in the case of its gradients, where small differences determine whether the gradient is positive or negative. Neglecting barometric pressure changes can lead to errors of order of magnitude for a dry adiabatic lapse rate of 0.1 K per 10 m, which is reasonable for such small distances.

However, such small vertical separation distances (below 10 m) are not recommended because the resulting temperature differences are small compared to the typical accuracy of temperature sensors (0.1 K). It might appear surprising, but due to radiation and turbulent heat fluxes, achieving better temperature measurement accuracy is challenging. On the other hand, too large a separation distance will diminish the accuracy of gradient approximation. Occasionally, especially at coastal locations, it can also cause the top measurement level to lie beyond the surface layer that may be as low as 20-m to 5- m. This is a much thinner surface layer than is typical for onshore locations.

In conclusion, for most small wind turbine site assessments, where having a 50-m to 100-m met mast is not an option, maximizing the temperature differences shall be a priority. For guidance, Figure 11 shows the histograms of temperature difference among different separation distances, while Figure 12 shows the corresponding differences of virtual potential temperature. Data were collected at Norwegian University of Science and Technology, NTNU Frøya wind measurement station during the years 2009 to 2015.

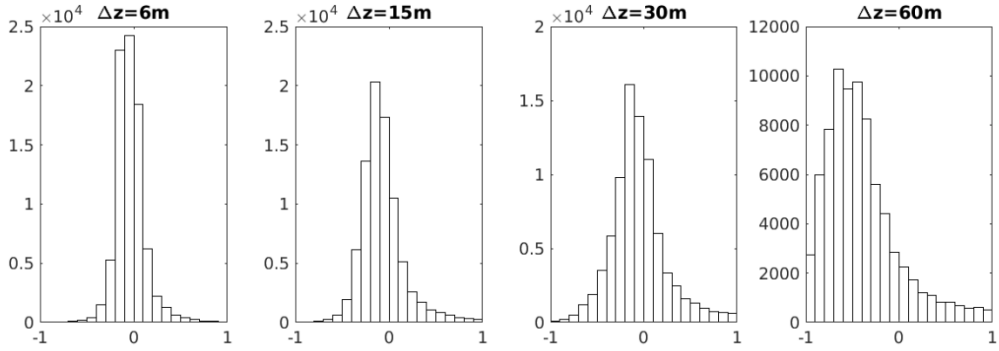

Figure 11. Histogram of temperature differences as a function of a vertical separation distance

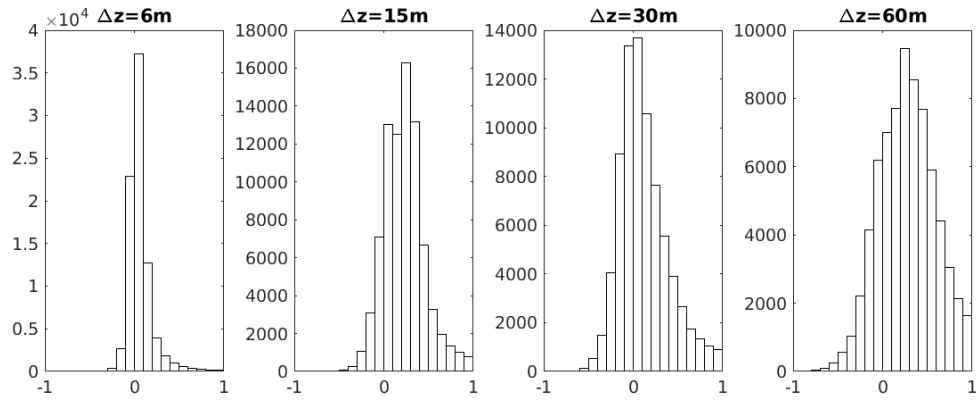

Figure 12. Histogram of virtual potential temperature differences as a function of a vertical separation distance

It is noticeable that the differences between T and θ_v grow rapidly with increased vertical separation distance, with opposite trends. While the temperature gradients are mainly negative, the gradients of virtual potential temperature are positive, which is due to high moisture content (presented data are from a coastal site in mid-Norway). At many wind energy sites, this will not be the case. In those situations, the largest contribution to calculating the local value of θ_y will be the pressure difference over Δz, which can reasonably be estimated by a surface or other reference height pressure and the mean temperature over Δz.

A second important parameter is important for the formation of coherent structures. The friction velocity u_* can be expressed as

$$u_* = \sqrt{\overline{u'w'}} \tag{6}$$

where u' and w' refer to the horizontal and vertical turbulent velocities measured by a three-dimensional ultrasonic anemometer, respectively. The friction velocity expresses the vertical momentum flux or, more accurately, the vertical transport of horizontal momentum. It is related to the Reynolds shear stress by the relation

$$\tau_w = \rho u_*^2 \tag{7}$$

where τ_w is the shear stress at the wall and ρ the mass density. The friction velocity u_* is proportional to or scales the *total* turbulent kinetic energy (TKE) in the flow and the Richardson number influences how that energy is spectrally distributed; i.e., the energy contained by eddy size. Eddy sizes whose dimensions are less than or equal to the turbine rotor diameter are the most important in creating unsteady aerodynamic-induced loading of the turbine blades.

When a sheared turbulent inflow to the turbine rotor is weakly stable, ($0 < Ri_g < 0.25$) Kelvin-Helmholtz shear Instability (KHI) may develop. Depending on the values of Ri_g and u_*, a range of sizes and intensities of spatially and temporally coherent vortices may be created. When a blade encounters these structures of near chord dimensions, a strong unsteady aero-elastic response can develop, which leads to increased dynamic loads and fatigue. The fatigue damage is

proportional to the friction velocity measured at hub height and is greatest within a critical stability regime defined by $0.01 \leq Ri_g < 0.05$.

2.3 Richardson Number Impacts

It is widely accepted that turbulence is a stochastic variation of a mean wind speed over time. This is easiest to translate by representing a resulting wind velocity magnitude as a sum of a mean wind speed and a fluctuating component. A suitable measure of the fluctuating component is the TI, defined by the IEC 61400-2 standard as $I = \sigma_U/U$, where σ_U is the standard deviation of the velocity and U the mean velocity, both taken over a suitable period (typically 10 minutes).

However, to express the impact of turbulence on wind turbine loads, turbulent flow of air is usually analyzed in the frequency domain by means of a power spectral density function such as, for example, the Kaimal spectrum. The Kaimal spectrum describes the contribution of different frequencies to the total variance of the wind speed. A larger turbulent structure has low-frequency variation in wind speed, while smaller vortices undergo short, high-frequency speed variations. Using generally accepted Taylor's hypothesis of frozen turbulence (Taylor 1938), in which the characteristics of eddies can be considered constant, or frozen, in time and vortices travel with the mean horizontal wind speed, the length and timescales of turbulence are connected. Assuming an eddy's characteristic size to be d (m) and its velocity to be U (m/s), its travel through a turbine rotor area would take $\tau = d/U$ seconds. At the same time, the frequency associated with this period is $f=1/\tau$ (Hz).

The typical length scales of high-energy, large turbulent coherent structures are in the range of several kilometres. These large eddies decay to smaller and smaller eddies as turbulent energy dissipates to heat. That way the change in underlying low-frequency, large vortices transitions to high-frequency small structures. Kolmogorov's law describes this process and states that the asymptotic limit of the spectrum is $f^{-5/3}$ at the high-frequency end.

The power spectrum of turbulence tends to be modified by the landscape. If the surface roughness of the landscape is high (i.e., urban terrain, peri-urban terrain or open terrain with ridges, hills, groups of high trees), the TI of air flow increases. Such land topography typically generates turbulent structures of the same length scale as that of the landscape "obstacle" itself, increasing energy (in the sense) at the corresponding frequency range. This shift in power to a higher frequency band (bin) has a detrimental effect on rotor fatigue loads. The more frequent the loads are, typically the shorter the life cycle of a wind turbine is. Another important aspect to consider is the atmospheric stratification. Neutral conditions are not so common, but the near-neutral conditions are typical for medium and high wind speeds (Petersen et al. 1998). These are the most important for fatigue damage calculation because they translate to an increased thermal convection from the ground up and vice versa depending on seasons and the time of a day (diurnal cycle).

Figure 13 shows the typical relationship between an A-B highly coherent structure and otherwise low coherent structure between points C-A or C-B. A very small high-frequency gust of one-third the size of a typical small wind turbine rotor blade length (eddy 2) passing through the rotor disc near Blade III, for example at 15 m/s, may have little effect on Blades I and II, especially when the turbine is variable speed controlled. On the other hand, a large gust of 30 m/s (eddy 2)

DRAFT

would have similar effects on all blades. The coherence of points A and B would be closely related, while at distant point C a low coherence with either A or B would be observed. In other words, low-frequency variations affect a larger area of the rotor than high-frequency variations.

Finally, it should be noted that through their rotary motion, the blades experience a different load spectrum than that of the Kaimal spectrum derived for a point in space. The blade will pass through any given eddy once in every revolution. In Figure 13b, an actual rotationally sampled load spectrum on Blade I differs from the Kaimal load spectrum for a point in turbulent inflow (Arany et al. 2014). If the size of both eddies is comparable, Blade I is rotating with a constant angular speed (or constant frequency f) and would pass through Eddy 1 and Eddy 2 once in each revolution. Therefore, when rotationally sampled, the wind speed load experienced by Blade I in the power spectral density plot will create peaks at the rotational frequency f_{1P} and at higher harmonics ($f_{2P}=2f_{1P}$, $f_{3P}=3f_{1P}$). This effect for a large structure coherent in A-B-C is more important for blade load analysis than a smaller non-coherent structure. Typically only higher order harmonics are transferred to the rotor-nacelle assembly as all blades pass through the same eddies. More information about spatial coherence and rotational sampling can be found in, e.g., Hansen (2008) and Veers (1988).

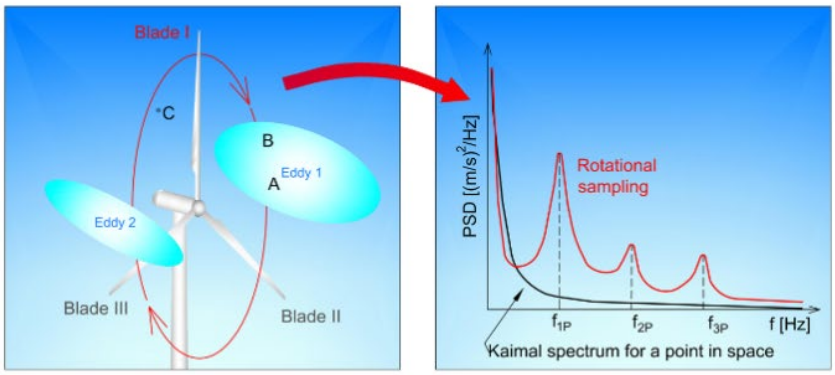

Figure 13. Importance of coherent structures' impact on rotor blades (Arany et al, 2014)

The unsteady structural response associated with encountering a coherent turbulent structure simultaneously excites many vibrational (modal) frequencies in the turbine blades as they pass through a rotor disc and are transferred into the drivetrain and turbine structure as flow-induced vibrations.

Thus TKE contained in a substantial coherent turbulent structure associated with each frequency sums up creating fatigue loads of high amplitudes manifested by increased stress on a turbine rotor, nacelle and an entire support structure. Conditions that produce coherent turbulent eddies can be destructive to wind turbines and decrease component life if frequently encountered.

3. TECHNICAL RECOMMENDATIONS FOR STRUCTURAL DESIGN

3.1 Vibration and Oscillation Assessment

As for all rotating machinery, small wind turbines are subject to self-excited oscillation and vibrations, which induce dynamic loads in various components of the turbine, including its support structure. While static loads calculation is a common practice that is generally taken into consideration when dimensioning foundations and towers for small wind turbines, the magnitude of dynamic loads is often underestimated when designing and planning a small wind turbine and its support structure. This has led to long-term failures and fatigue damage of rotor components and towers in the past.

3.1.1 Resonance of Oscillating Structures

Oscillation amplitude assessments of several small wind turbines in the Energy Research Park in Lichtenegg, Austria, have shown that resonant oscillations stimulated by intrinsic rotor oscillations occurring at specific rotational speeds are the main reason for increased vibrations and dynamic loads.

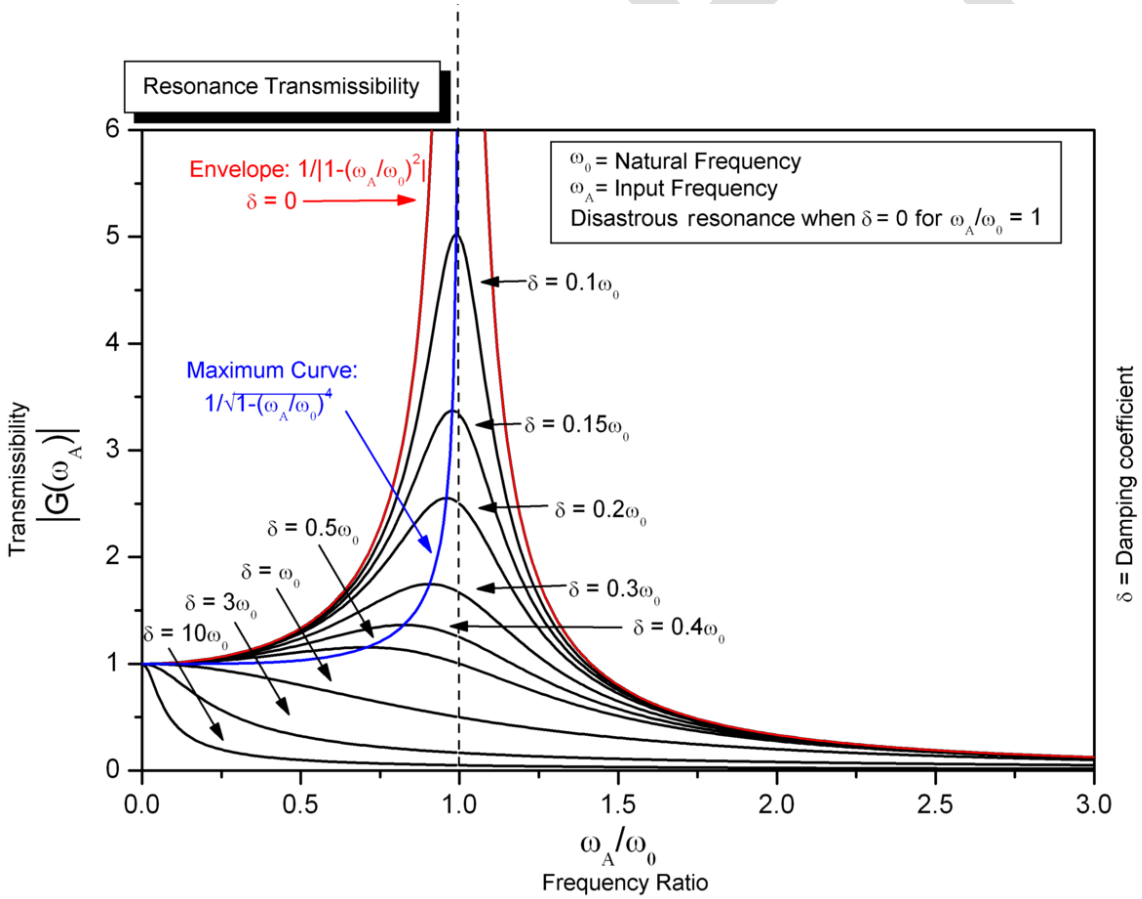

Figure 14. Magnitude of oscillations at resonance as function of damping factor (Ajoy Ghatak 2005). Optics, 3E (3rd ed.). Tata McGraw-Hill. p. 6.10. ISBN 978-0-07-058583-6

Each mechanical or structural component of a small wind turbine, including the tower or supporting structure, has several natural frequencies that vary in relation to the size, shape, and material of the component. As natural frequencies may shift when altering the dynamic characteristics of the supporting structure or a component of the turbine, it is crucial to identify natural frequencies for each application.

In this case, the driving forces of the exciting oscillation are not dissipated in the structure but stored and accumulated in the form of oscillating energy. During each oscillation period, oscillation energy is accumulated in the structure, up to the point where the energy dissipated by the structural damping is equal to oscillation energy induced by the rotor. This means that in case of resonance, the only parameter limiting the oscillation amplitude is the structural damping factor of the oscillating system. As shown in Figure 14, the dynamic forces f_R induced into the system in a resonance situation can be several times higher as compared to a non-resonant operation range for structures with low damping factor D.

$$f_R = \frac{1}{2D \times \sqrt{1-D^2}} \quad (8)$$

For classic steel towers that typically have a structural damping factor around 2 %, the magnitude of a resonant oscillation can be 50 times higher than in normal operation. These excessive loads are often not considered during design and installation of small wind turbines and can be a cause for failures. To reduce the risk of fatigue failure, the following approaches are recommended:

- Small wind turbine tower systems should be designed in a way that guarantees an overcritical mode of operation within the range of 70 % P_N to full rated power when stimulating forces are relatively high.
- Small wind turbine tower systems should be designed to have as high a structural damping factor as possible. Damping factors between 10% and 20% are desirable. To increase the structural damping and reduce natural frequencies, damping or decoupling elements may be used.
- In regards to small wind turbines, resonances are likely to occur within the tower-rotor system as the natural frequency of these structures (several meter high tower with high rotor mass on top) often fall in the critical frequency range matched by the rotor at high wind speeds.

Table 3. Typical Stimulating Oscillation Orders

Oscillation Source	Frequency/Order
Rotor imbalance	$1\times f_{RPM}$
Drive shaft misalignment	$2 \times f_{RPM}$
Blade passing frequency	$n_{blade} \times f_{RPM}$
Harmonics of blade passing frequency	$X \times n_{blade} \times f_{RPM}$
Generator pole passing frequency	$n_{pole\ pair} \times f_{RPM}$
Harmonics of generator pole passing frequency	$X \times n_{pole\ pair} \times f_{RPM}$
where f_{RPM} is the rotation frequency (Hz), n_{blade} the number of rotor blades, and n_{pole_pair} the number of generator pole pairs	

3.1.2 Structural Damping Factor as Key Parameter

Stimulating oscillations of the first 10 orders are particularly critical as their relatively low frequency compared to generator induced oscillations translates into relatively large displacements, leading to high loads and stress in the structure. Additional stimulating oscillation orders not listed in the table may arise (depending on turbine design) as interactions between rotor blades or aerodynamic effects may result in complex resonant vibrational modes in the rotor.

Despite the fact that IEC 61400-2 suggests a Campbell analysis be performed for the wind turbine, the standard lacks effective recommendations regarding how to handle increased oscillations detected in order analysis.

3.1.3 Recommended Countermeasures

Defining general limit values for maximum oscillation amplitudes is not possible as turbine designs and RPM ranges vary between manufacturers and have a big impact on this value. Therefore, we suggest using minimal structural damping factors that should be reached by turbine-tower combination design. To identify the structural damping factor, a modal test should be performed. The damping factor can be determined by measuring the reduction of the oscillation amplitude from one period to the following, as shown in Figure 15. With this method, damping factors between 10% and 20% should be reached to limit resonant oscillation. On top of that, designs having natural frequency within a range of rotational speeds for which a turbine achieves between 70% and 100% of its rated power should be avoided. In case a natural frequency appears to fall in this critical range, adapting the tower design or installing damping elements can tune the system's natural frequency to be matched at lower wind speeds or outside the operational range of the turbine.

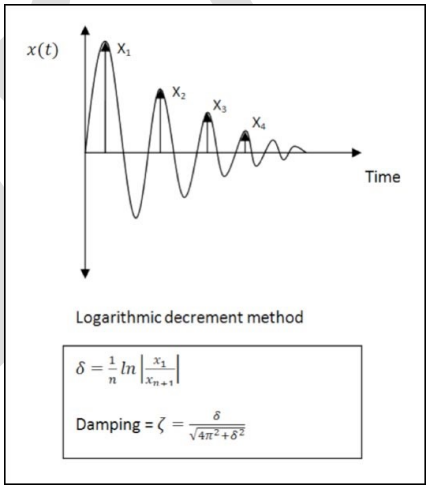

Figure 15. Logarithmic damping decrement determination

(Porter McGuffie Inc, Damping Evaluation, last opened 15.09.2018, http://pm-engr.com/damping-evaluation-2/)

In case a design adaptation isn't possible and/or a damping factor of 10% to 20% can't be achieved by the design, an adaptation in the turbine controls should be performed to avoid

critical RPM ranges in which resonances might occur. This can be done by reducing or increasing generator loads when the rotor is running at critical RPM to accelerate or decelerate the rotational speed. But care should be taken because the turbine rotor could "stick" in the critical RPM during deceleration. This effect is aggravated by the fact that oscillating systems tend to preserve the state of resonance. The reason is that when there is resonance, a part of the rotating energy is transduced into oscillation energy, which tends to keep the RPM constant.

3.2 Assessment of SWT Structural Component Fatigue Damage

The majority of SWT installations take place in the lowest layer of the atmosphere where turbulence characteristics vary both diurnally and with height above the ground. For example, the variation of wind speed with height or wind shear varies strongly over the diurnal cycle due to the heating and cooling of the earth's surface. During the day, the sun heats the ground, causing the air to become buoyant and resulting in currents containing spatially *large* rising and sinking air motion circulations called turbulent eddies. This *convective* process warms the air above the ground with the warmest air at the surface and with the temperature decreasing with increasing height. Such conditions are referred to as being *stable, unstable and neutral*, as shown in Figure 16.

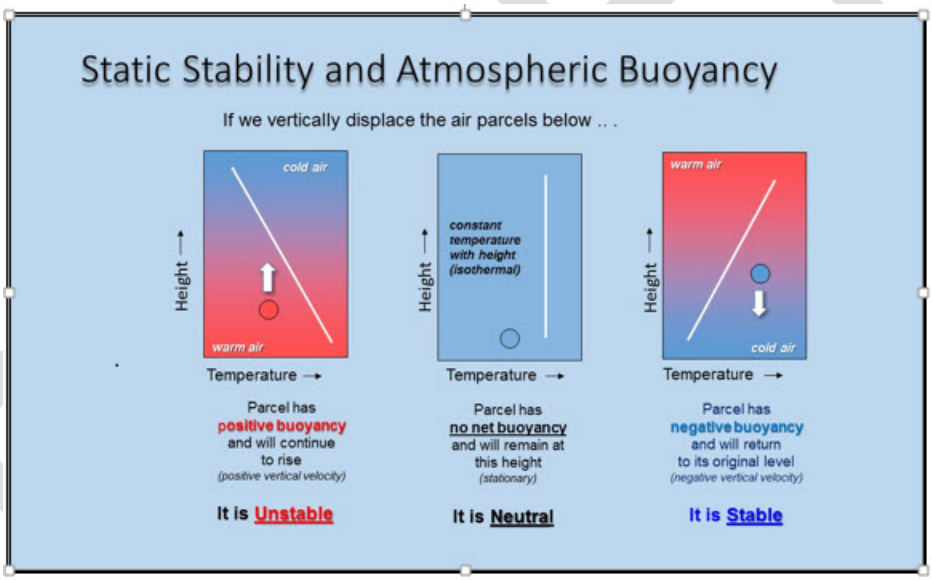

Figure 16. Static stability (diagram courtesy of Neil Kelley)

Late in the afternoon, when the sun is lower in the sky, the rate of heating of the ground decreases with the lowering of the sun until, at some point just before sunset, it stops warming and begins to lose heat through radiation. This cooling of the ground surface increases more rapidly after sunset. The air near the surface begins to be cooler than the air above it, with the thickness of this cooler layer increasing during the night. Under such conditions, the turbulent eddies *become much smaller* due to the damping (capping) action of the presence of warmer, less dense air above. This damping action is associated with what are referred to as *stable* conditions with the air temperature increasing with height. Should the air temperature become constant with

height, such conditions are known as *neutrally* stable. The lower atmosphere tends toward neutral stability when strong winds are present.

Research over the past 20-plus years has shown that the periods of greatest structural fatigue damage occurring on operating small wind turbines also exhibits a diurnal variation with the most damage often taking place near local sunrise and again during the late afternoon and early evening hours. It was therefore found that the *vertical stability* of the atmospheric layer from just above the ground to the maximum height of the turbine rotor played a significant role in the turbine's fatigue damage accumulation. Therefore it is a major contributor to the reduction of the observed lifetimes of structural components of a small wind turbine installation in a specific operating environment.

Currently the turbulent operating conditions for small wind turbines are specified by the *turbulence intensity parameter* I_{15} given by the dimensionless ratio of the standard deviation of the hub-height *horizontal* wind speed σ_U to the mean speed or σ_U/U where U is 15 m/s. The value of I_{15} is fixed at 0.18 for all small wind turbine design classes with the exception of Class S. Further neutrally stable conditions are assumed to exist as well. The distribution of turbulent spectral energy or NTM is quantified by the IEC-scaled versions of the Kaimal or Mann spectral models. Direct, synchronized measurements of the properties of the turbulent inflow and the corresponding response of a series of turbine aeroelastic and structural parameters were gathered for three small wind turbine designs. It was found that the observed fatigue damage scaled with both the vertical stability as described by the gradient Richardson number (*Ri*) of the atmospheric layer occupied by the turbine and its tower and the turbulent shearing stress u_* measured by a three-dimensional sonic anemometer at hub height.

3.2.1 Richardson Number Stability Parameter

The spectral distribution (eddy sizes) of atmospheric boundary layer turbulence varies with the vertical stability of the layer being measured. Under unstable or convective conditions, *positive buoyancy* creates turbulent eddies that are very large, often with spatial dimensions of 1 to 3 km in both the horizontal and vertical. In contrast, when the atmospheric layer is stable, *negative buoyancy* causes the atmosphere to become *vertically stratified into numerous shallow layers*.

Under the damping action of the negative buoyancy, the turbulent eddy sizes become much smaller and the dimensions often are larger horizontally than vertically because of the limiting heights associated with the individual stratified layers. Thus the impact on the aerodynamic loading of turbine rotor blades is associated with the time and amplitude of variation in the aerodynamic lift and drag as a turbulent eddy is ingested; i.e., turbulence-induced unsteady aerodynamic loading. In unstable flows with the large eddies encountering the rotor, aerodynamic responses that are much less abrupt are created because the induced changes in the attack angle are smaller and take much longer to move through the rotor disc. Contrary to this is a situation in stable flows in which the small eddies induce larger attack angle fluctuations, resulting in larger and more intense lift and drag variations.

The Richardson number stability parameter (*Ri*) is defined as the ratio of turbulence created or suppressed by buoyancy to that generated by vertical wind shear. Negative values of *Ri* correspond to unstable conditions, positive ones stable and zero neutral. The *Ri* measured over

the layer from near the ground to the top of the turbine rotor disk is indicative of the distribution of the spatial organization, sizes and strengths of turbulent eddies being ingested by an operating small wind turbine rotor. While it is possible to ascertain a measure of the stability of the atmospheric layer in which the small wind turbine resides by using the vertical wind shear, the *Ri*'s relationship to the development of coherent turbulent structures (KHI) makes it more useful as a scaling parameter for structural loading and fatigue damage accumulation.

The simplest direct measurement of the vertical stability is the bulk Richardson number, Ri_B is given by

$$Ri_B = \frac{9.8(T_2 - T_1)(z_2 - z_1)}{0.5(T_2 + T_1)(U_2 - U_1)^2} \tag{9}$$

where T_2 and T_1 are the mean absolute temperatures (°K) and wind speeds measured at heights z_1 and z_2 or $T(z_1)$, $U(z_2)$ and $T(z_2)$, $U(z_1)$. The height z_1 is near the ground (nominally ~ 2m) and z_2 corresponds to the maximum elevation of the small wind turbine rotor. The air temperatures are measured at each of these heights within naturally aspirated radiation shields.

3.2.2 Mean Shearing Stress or Friction Velocity

In the atmospheric surface boundary layer, the vertical transport of momentum or shearing stress is given by $u_* = \sqrt{u_1' u_3'}$ where u_1 and u_3 are the streamwise (parallel to the axis of turbine shaft) and vertical fluctuating turbulent (zero mean) wind components. The value of u_* scales the energy contained within the turbulent wind spectrum; i.e., the larger the value of u_*, the more energy is contained in the turbulent eddies.

*3.2.3 Scaling of Fatigue Damage Equivalent Loads with Ri and u**

Figure 17a shows the variation of the three-blade average damage equivalent load (DEL) as a function of *Ri* for two adjacent Micon 65/13 wind turbines, while Figure 17b displays a contour plot of the variation of the DEL with both *Ri* and u_*. Unstable conditions are shown as $Ri < 0$, neutral at $Ri = 0$ and stable as $Ri > 0$. Figures 17a and 17b illustrate that the maximum fatigue damage is associated with high values of u_* and *slightly or weakly* stable conditions and not neutral nor convective (unstable).

The most damaging fatigue loads have been found to occur within the weakly stable range of $+0.01 \leq Ri < +0.05$, with the maximum damage seen at a value near +0.02. The u_* also typically reaches a maximum within this same narrow stability range. Field measurements of the time-varying turbine structural response have been time-correlated with turbulent properties in the inflow derived from three-dimensional sonic anemometers. It has been found that the short-period (less than a single blade rotation) dynamic loading of turbine blades is a consequence of the rotor ingestion of spatially and temporally organized or *coherent* turbulent structures. These organized turbulent patches are superimposed on or embedded within the wind flowing through the turbine rotor disk. Such coherent structures occur most frequently and are most intense within the same weakly stable range of $+0.01 \leq Ri < +0.05$ and are the source of much of the greatest fatigue damage.

DRAFT

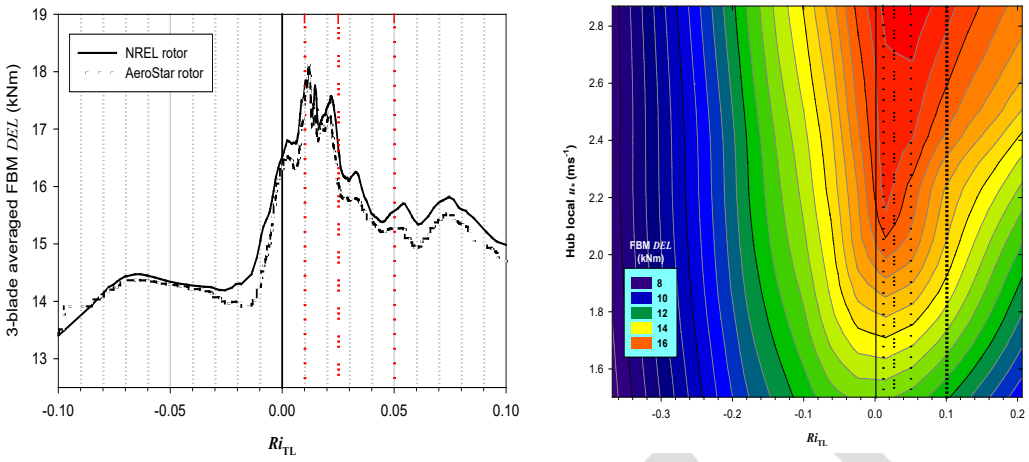

Figures 17a and b. Measurements show the variation of blade root flapwise bending moment DEL of two adjacent Micon 65/13 turbines with Ri stability. Vertical dot-dash (Ri = 0.01) and dash-dot-dot (Ri = 0.025) lines delineate maximum response region with dash line (Ri = 0.05) indicating the upper limit of stability-influenced response; (b) Variation of blade root flapwise bending moment DEL with Ri and u*.

3.2.4 Characteristics of Turbulence-Induced Loading

The fatigue damage accumulation on small wind turbine structural elements arises from the *cyclic* loading seen from the effects of the rotor rotation within the gravity field and the variation of wind speed with height (wind shear). Superimposed on the cyclic load cycles are intense, short-period loading events that take place within a small sector of the rotor disk. These latter events being impulsive in nature are often more damaging than a load cycle that occurs over the period of one rotor rotation or more. Research has found that rotor blades encountering coherent turbulent structures are responsible for inducing strong, short-period unsteady structural responses resulting from the transient stalling of the blade, which lead to impulsive load excursions and potentially shorter component life if strong and frequent enough. Figure 18 presents an example of the details of the turbulent processes involved in the damaging fatigue response seen in this narrow stability range (discussed in Sections 6 and 7 of Kelley 2011).

DRAFT

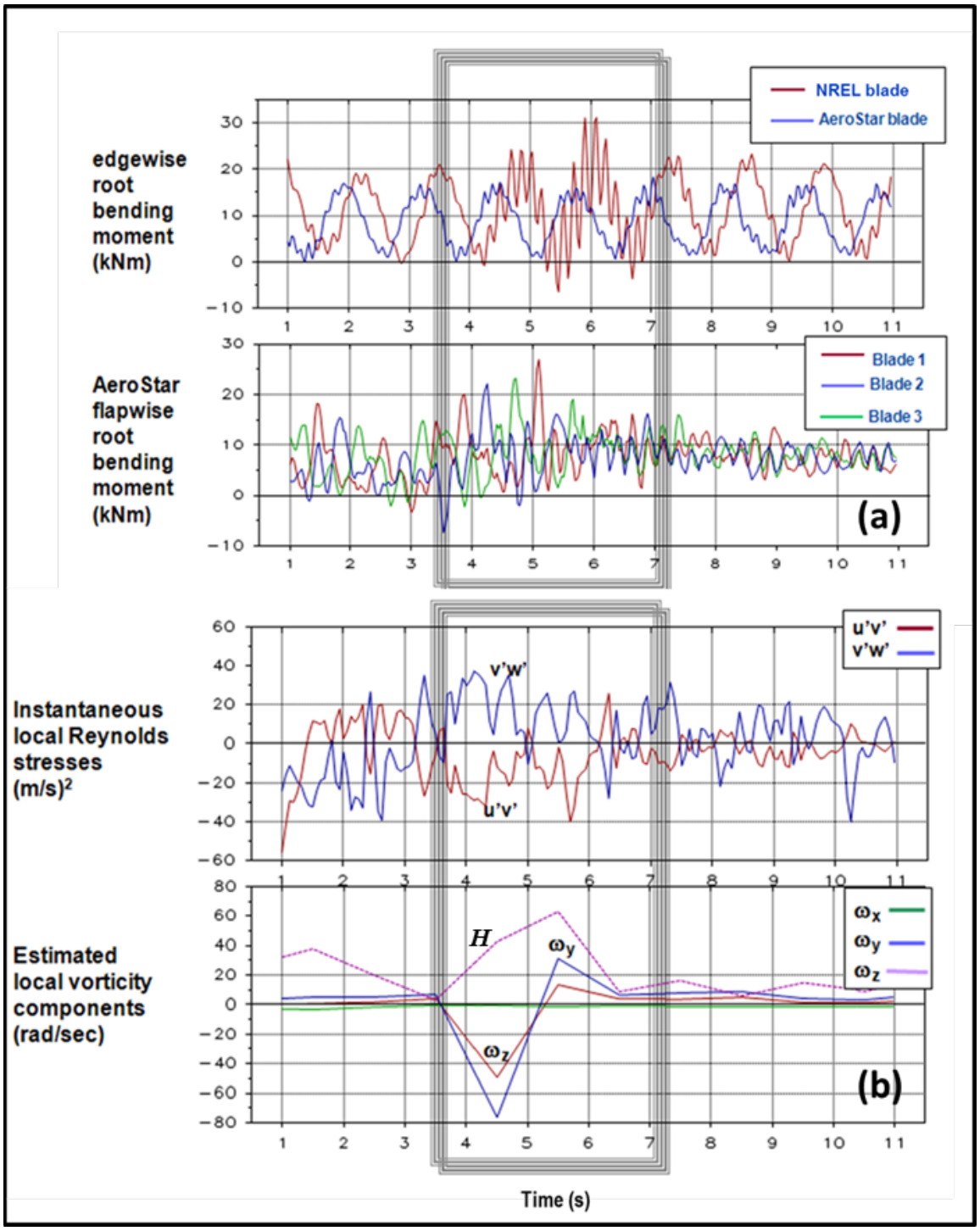

Figure 18. Significant loads seen on Micon 65/13 NREL and AeroStar rotors: (a) load excursions in flapwise and edgewise root loads; (b) corresponding instantaneous u'v' ($u_1'u_3'$) and v'w' ($u_2'u_3'$) Reynolds stresses and estimated local vorticity components ωy and ωz. H is the local relative helicity, a measure of the spatial intensity of the rotational spin of the structure. A coherent turbulent structure exists in the flow between about 3 and 6.5 seconds to which the turbine rotors responded

Figure 19 displays examples of short-period or impulsive flapwise bending moment (FBM) loads occurring on each of the three blades of a Micon 65/13 turbine. Note that (1) these loads occur during the descending clockwise motion of the blades, and (2) that a single larger and more intense load peak occurs on Blade 3 under slightly more stable flow conditions; i.e., Ri = +0.034 as opposed to Ri = +0.007. Measurements of other horizontal-axis wind turbines have confirmed that blade peak FBM loads most frequently occur when the blades are descending and within ±25-30° of the horizontal.

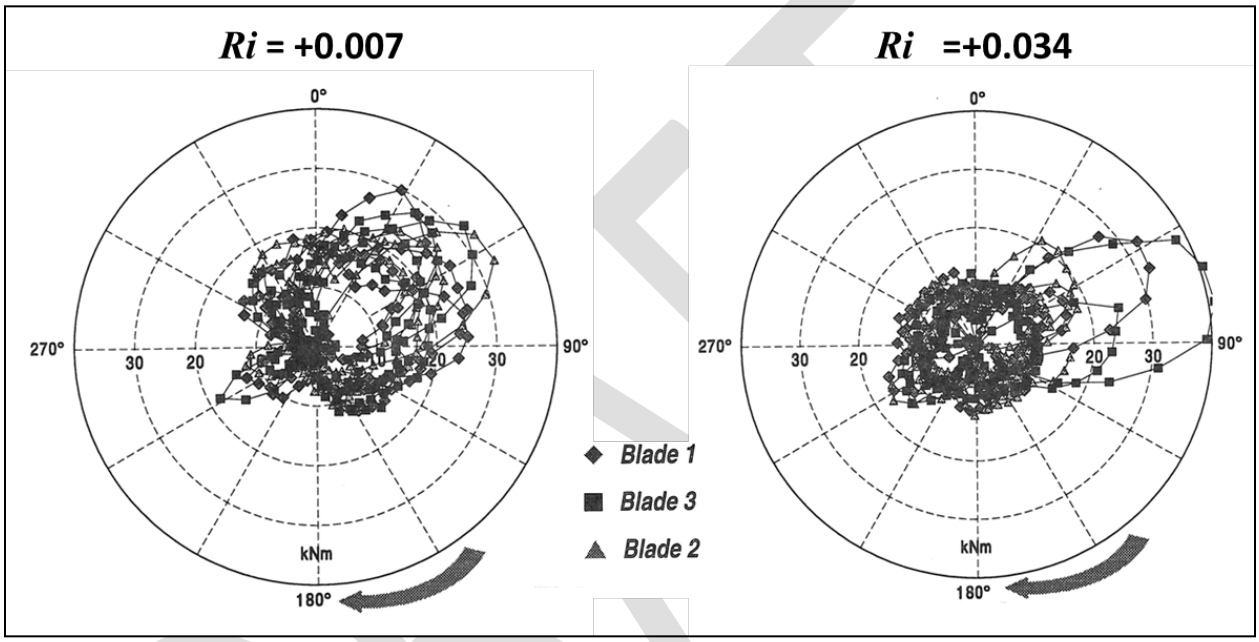

Figure 19. Polar plots showing the azimuth locations of instantaneous FBM load excursions in kNm occurring on each blade

3.2.5 Origins and Characteristics of Coherent Turbulent Structures

The turbulent coherent structures responsible for the aeroelastic rotor responses seen in Figures 17a and 17b, and 18 are a product of a type of an atmospheric flow instability that most often occurs during the night-to-day and day-to-night transitions of the atmospheric boundary layer. During these periods, the vertical stability goes from stable to unstable in the morning and the reverse in the evening. During these transitions, the boundary layer flow in which the small wind turbines are immersed is weakly stable; i.e., nominally within the range $0 < Ri < 0.1$. It is during these weakly stable periods that the conditions for a form of flow instability called KHI can develop and persist. It is this KHI that is responsible for the development of the intense coherent turbulence structures being ingested into small wind turbine rotor disks. Typically KHI conditions persist longer during the day-to-night boundary layer transition than is seen in the morning hours.

Currently as shown in Equation 1 in the IEC 61400-2 standard, the turbulence level in the turbine inflow is specified in terms of the *turbulent intensity* at hub height, given by the ratio of the

standard deviation of the streamwise wind component to the mean value or $I = \sigma_1/V_{hub}$ measured by an IEC-certified cup anemometer at hub height. A characteristic value of $I_{15} = 0.18$ is specified for all turbine classes. The corresponding value of σ_1 is shown in Equation (1).

For the IEC NTM, the crosswind or lateral and the vertical wind component standard deviations are specified as $\sigma_2 = 0.8\sigma_1$ and $\sigma_3 = 0.5\sigma_1$ as a measure of the intensity of the turbulence in the turbine inflow. For the most rigorous small wind turbine Class 1 design conditions, the values are $\sigma_1 = 2.1$, $\sigma_2 = 1.68$ and $\sigma_3 = 1.05$ m/s.

The *total* TKE contained in a representative flow entering a small wind turbine rotor at hub height is defined as:

$$\text{TKE} = \sigma_1^2 + \sigma_2^2 + \sigma_3^2 = u_1'u_1' + u_2'u_2' + u_3'u_3' \tag{10}$$

where the primed quantities represent fluctuating (zero-mean) value of the wind component velocities. The TKE value for the IEC small wind turbine class discussed above is 8.335 m^2/s^2. TKE is the sum of *homogenous isotropic* turbulence (E_{iso}) (invariant of spatial position) and anisotropic or *coherent* turbulent kinetic energy (CTKE), which exists as definite temporal-spatial organizational elements in the flow. CTKE is defined in Equation 11, as measured by a three-dimensional ultrasonic anemometer:

$$\text{CTKE} = 1/2[(u_1'u_3')^2 + (u_1'u_2')^2 + (u_2'u_3')^2]^{1/2} \tag{11}$$

thus

$$\text{TKE} = E_{iso} + \text{CTKE}. \tag{12}$$

The intensity of organized, coherent turbulent structures in the turbine inflow can be described by the value of CTKE associated with them. Research has found that such structures are *exponentially distributed* in time and can be modeled as an inhomogeneous Poisson process. Figure 20 shows the temporal and spatial distribution of coherent turbulent structures measured by both a LiDAR and vertical mast-mounted three-dimensional sonic anemometers in a nocturnal, weakly stable boundary layer over flat relatively homogenous terrain. While most small wind turbines are installed at heights below 40 m, some of the organized bursts of TKE shown in Figure 20 extend to the altitudes that would impact the small turbine rotor. Typically in a nocturnal boundary layer such as this, the CTKE is being transported toward the ground surface and thus into the inflows of small wind turbines installed nearer to the ground.

3.2.6 Impact of Coherent Turbulence on Small Wind Turbine Aeroelastic Response and Fatigue Damage

The distribution of load cycles within a 10-minute record can be fitted with a mixed distribution model, as shown schematically in Figure 21. The high numbers of low amplitude and less damaging cycles are Gaussian distributed while the most damage is associated with fewer cycles with higher amplitudes that are exponentially distributed (note that the Y axis is in logarithmic scale). Figure 22 plots measured distribution of P-P root FBM cycles for the AWT-26 prototype wind turbine.

DRAFT

Figure 23 depicts contours of the maximum DELs associated with a 10-minute record as a function of *Ri* and hub peak values of CTKE. It is no accident that both the number and intensity of coherent structures and associated loading cycles are exponentially distributed. An analysis of the fatigue damage associated with CTKE peak amplitudes found that the largest damage occurs with values of 10 m^2/s^2 or greater with moderate and threshold levels occurring at 5 and 2 m^2/s^2 respectively.

Figure 24 plots the low-scatter, monotonic increase of the out-of-plane bending moments DELs in function of the logarithmically tallied hub peak CTKE values from more than 7,000 10-minute records measured on the National Wind Technology Center's 600-kW ART turbine. An exponential growth of bending moments is noticeable with an increase of TKE contained in coherent structures.

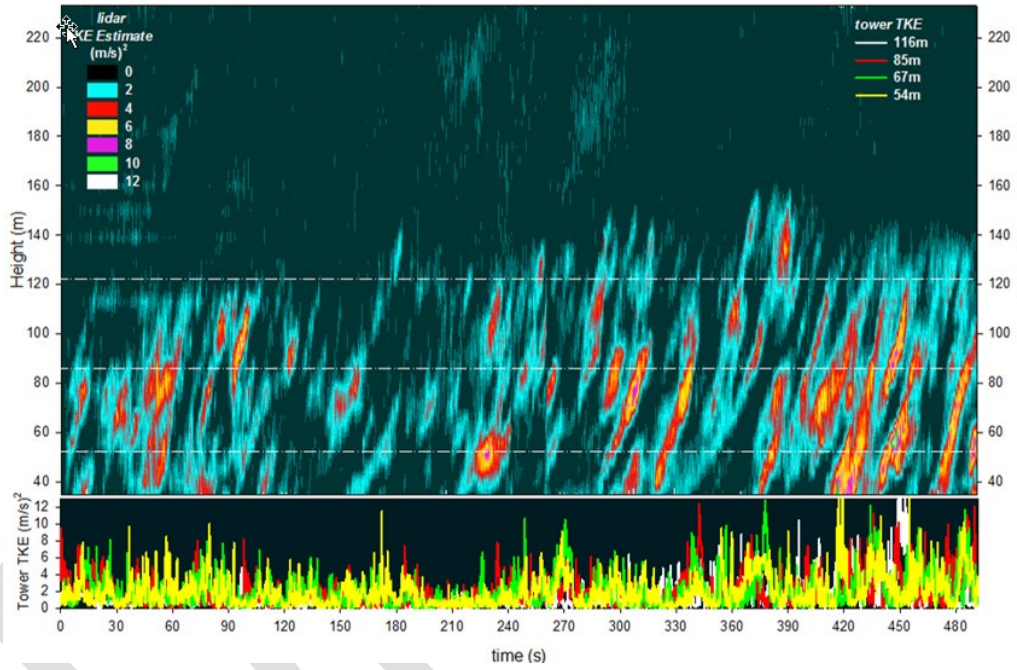

Figure 20. Lidar-estimated and mast-mounted sonic anemometer observations of organized bursts of TKE in a weakly stable atmosphere over flat and relatively homogenous terrain

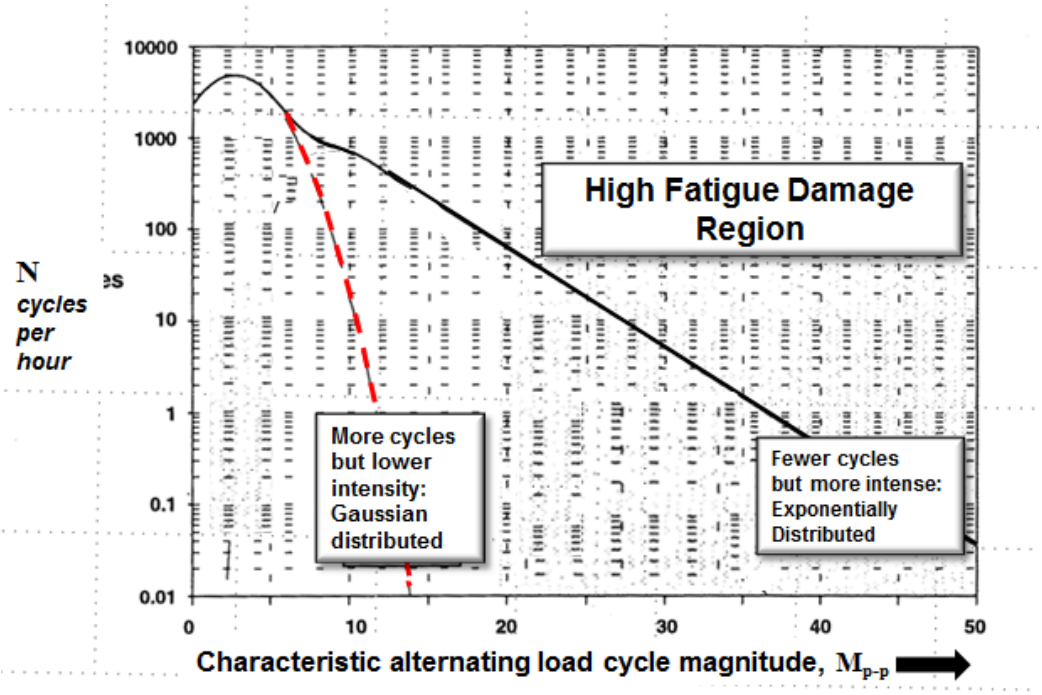

Figure 21. Schematic of relationship of high-frequency, low-amplitude Gaussian stress cycle distributions with lower-frequency, high-amplitude exponentially distributed stress cycles

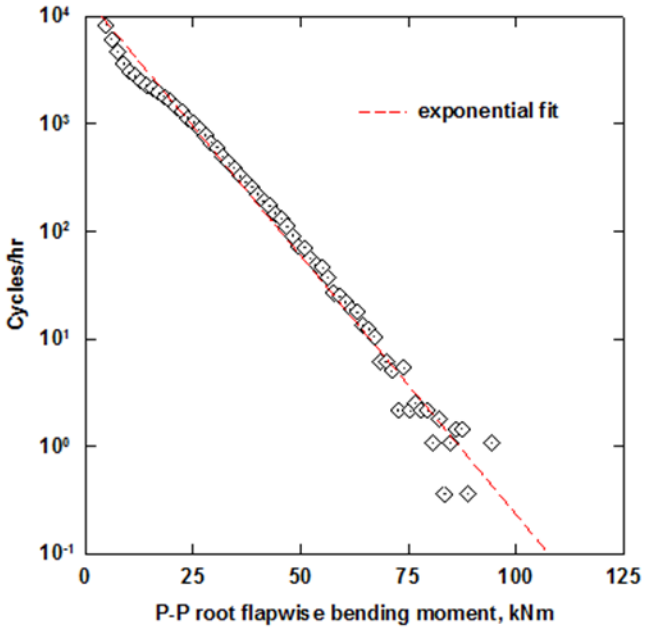

Figure 22. Example of measured root flapwise bending moment spectrum from AWT-26 turbine installed in Tehachapi Pass, California

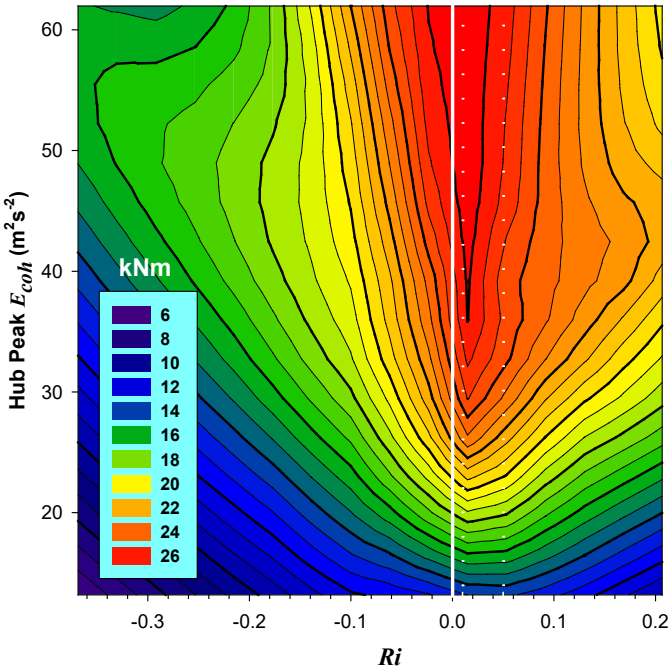

Figure 23. Variation of National Renewable Energy Laboratory (not NWTC like other references?)-rotor-equipped Micon 65/13 three-blade peak root FBM *DEL* with hub peak CTKE. Negative values of Ri_{TL} indicate dynamically unstable, zero neutral and positive stable flow conditions. Dashed lines outline the range of *Ri* where the greatest fatigue damage occurs, +0.01 < *R*i < +0.05

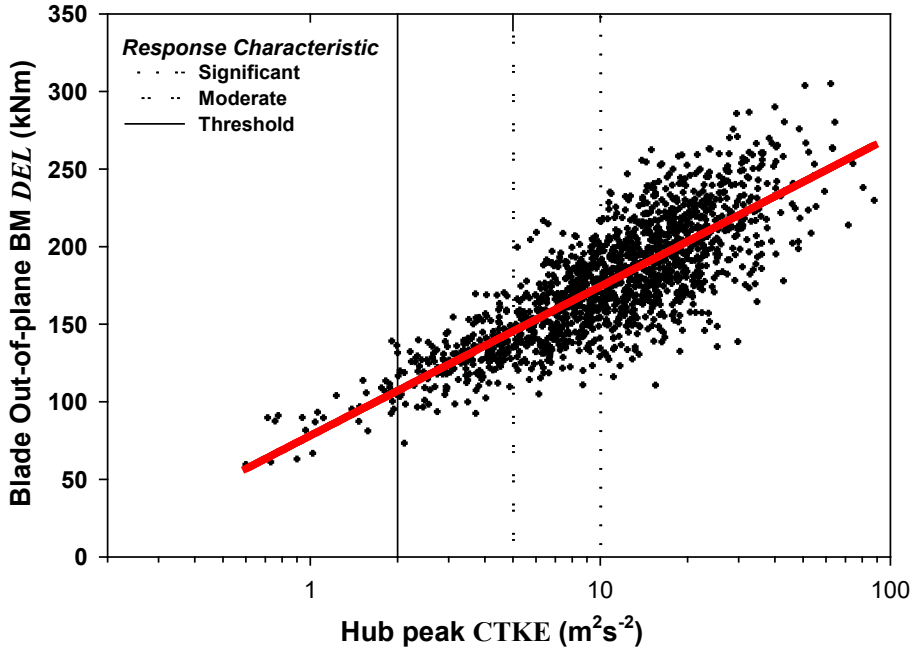

Figure 24. Variations of the NWTC ART root bending moment *DEL* with hub-height peak CTKE

3.2.7 Incorporating Non-Neutral Turbulence into the SWT Design Process

Figure 3 in the IEC 61400-2 Small Wind Turbine standard demonstrates the importance of simulation modeling in the turbine design process. Using a simplified loads methodology is not adequate to produce robust small wind turbine designs that must operate in a very wide range of turbulent inflows. Thus, simulation modeling used in tandem with loads measurements are required to produce safe, efficient and low-maintenance machines for the small wind market.

There are two simulation approaches that can be used to drive aeroelastic models. One is stochastic simulation, which is statistics based and produces a frozen sample of a spatial turbulent flow that is then time-stepped through the rotor to obtain the aerodynamics and mechanical responses of the simulated turbine. The other is to use a CFD model that produces a time-varying turbulent wind field to drive the simulated turbine rotor. To date, the engineering design process has mostly used the former approach, in which a stochastic simulation of the IEC NTM is used as the basis for determining the structural response of turbine design.

In principle, a CFD simulation of the fully coupled fluid-structure interaction simulation of a wind turbine under non-neutral turbulent conditions is possible. However, at present the computational cost of such a simulation would be prohibitive.

Several companies offer CFD modelling services. Two recommended practice documents for CFD simulation in urban environments are COST Action 732 (Best Practice Guideline for the CFD Simulation of Flows in the Urban Environment) and AIJ Guidebook (AIJ Benchmarks for Validation of CFD Simulations Applied to Pedestrian Wind Environment around Buildings).

The stochastic simulation approach, while not truly time-varying, lends itself to assessing the aeroelastic response of wind turbines in a probabilistic sense. Many fewer computational resources are needed to statistically assess predicted component lifetimes under known rigorous loading conditions and be validated by actual full-scale field measurements. Under this scenario, it is very important to isolate those conditions and to insure the simulated turbulent inflow incorporates them.

The IEC NTM approach with its four load classes makes an attempt to provide for design environment that is increasingly more challenging. This is done by step increases in the mean hub-height wind speed and associated turbulence level of a stochastic wind field. This simulated turbulent wind field is based on conditions seen over flat, homogenous terrain under neutral stability. When coupled with an aeroelastic simulation of a design turbine, it is an excellent first step to assess early design tradeoffs. However, to take into account the much wider range of turbulent conditions seen in the true world of operating environments, a much more realistic inflow structure and its impact on wind turbine dynamics is required. Research conducted by NREL over the past 20-plus years has been targeted to answer this question.

Detailed measurements of characteristic small wind turbine turbulent inflows have been taken in several distinct operating environments that have been synchronized with a wide range of engineering measurements. This work has allowed the identification of atmospheric flow conditions that are the most mechanically damaging to wind turbines and their component structures. The objective of this research has been to use this knowledge to develop a simulation

capability of such important conditions that can be used as a design tool in the development of new turbine designs. The turbulence characteristics so identified have been incorporated within the capabilities of the TurbSim Stochastic Turbulence Simulator. This simulator has been designed primarily to provide the wind input to the suite of computational codes developed and used by NREL's National Wind Technology Center (NWTC) principally interfacing with its FLAP Code through its aerodynamic routine Aerodyn. AeroDyn has been previously successfully integrated with the ADAMS® and Simpack multi-body simulation codes.

3.2.8 Identifying the Most Damaging Inflow Turbulence Characteristics

Time synchronized field measurements of the inflow turbulence and the corresponding turbine dynamic responses were acquired upwind, within and downwind of a 41-row California wind farm and upwind of the NWTC ART experimental turbine on Row 4 of the NWTC. Further extensive turbulence boundary layer measurements were acquired at a site on the high plains of Southeast Colorado but without the presence of a companion wind turbine. Each of these operating environments have particular characteristics, which have been quantified and included in TurbSim as suggested Special (S) cases (i.e., S1, S2, S3, S4, S5 and S6). Collectively they represent a very wide range of turbulent conditions that small wind turbines are likely to encounter.

Correlations between the turbulent properties of the turbine inflow and the turbine aeroelastic response found that the stability (as expressed the turbine layer Ri_{TL}) exhibited the most sensitivity. Further, this sensitivity could be expressed in terms of five ranges of the *Ri* parameter that we have designated as STC02, CRR, CRRH, STC04 and STC05 (see details in Kelley 2011) and which are listed in Table 4.

Table 4. Stability Classes

Stability Class Designation	Range
Moderate to Slightly Unstable Class, STC02	$-1 < Ri_{TL} \leq 0.00$
Weakly Stable Critical Range, CRR	$+0.01 \leq Ri_{TL} < +0.05$
Weakly Stable High Range Critical, CRRH	$+0.05 \leq Ri_{TL} < +0.10$
Moderately Stable Range, STC04	$+0.10 \leq Ri_{TL} < +0.25$
Very Stable Range, STC05	$+0.25 \leq Ri_{TL} < +1.0$

The greatest fatigue damage was found to reside in the CRR (**C**ritical ***Ri*** **R**ange shown in Table 4. The distributions of blade root flapwise bending DEL variation with stability class are shown in the boxplots of Figure 25.

The turbulent conditions within the CRR stability range from the three wind farm locations, the NWTC Row 4 and the Great Plains Site are compared as boxplot probability distributions in

Figure 26 a,b. The corresponding values for the IEC Class 1 NTM are shown on each graph. Clearly the conditions at Row 37 of the wind farm are severe and exceed the IEC values significantly, particularly for the vertical wind component u_3 (w). Compared with Row 37 in the wind farm, the turbulence is somewhat less severe at the NWTC on Row 4 while it is significantly less at the Great Plains Site. The turbulence conditions on Rows 37 and 41 of the wind farm and at Row 4 of the NWTC are frequently much more severe than is called for by the IEC Class 1 NTM. In comparison, the turbulence conditions at the Great Plains Site, while generally much less severe, do see strong but less frequent high-turbulence structures, as evidenced by the number of > P90 events.

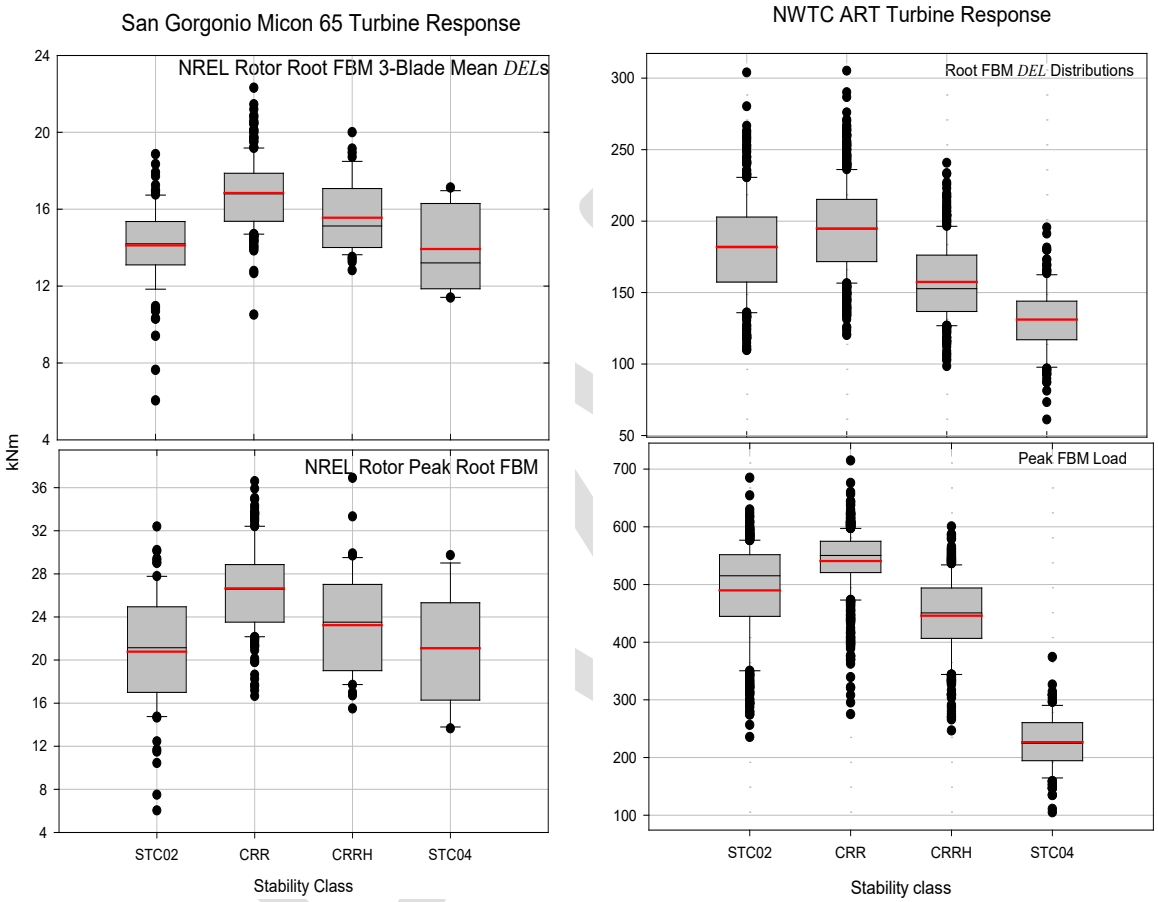

Figure 25. Boxplot probability distributions of observed root FBM DELs and peak load responses by stability class for the California Micon 65 and the NWTC ART turbines. The rectangles define the P25-P75 probability range while the black and red lines indicate the median and mean respectively. The "whiskers" mark the P10-P90 probability range and the dots represent events occurring beyond those limits

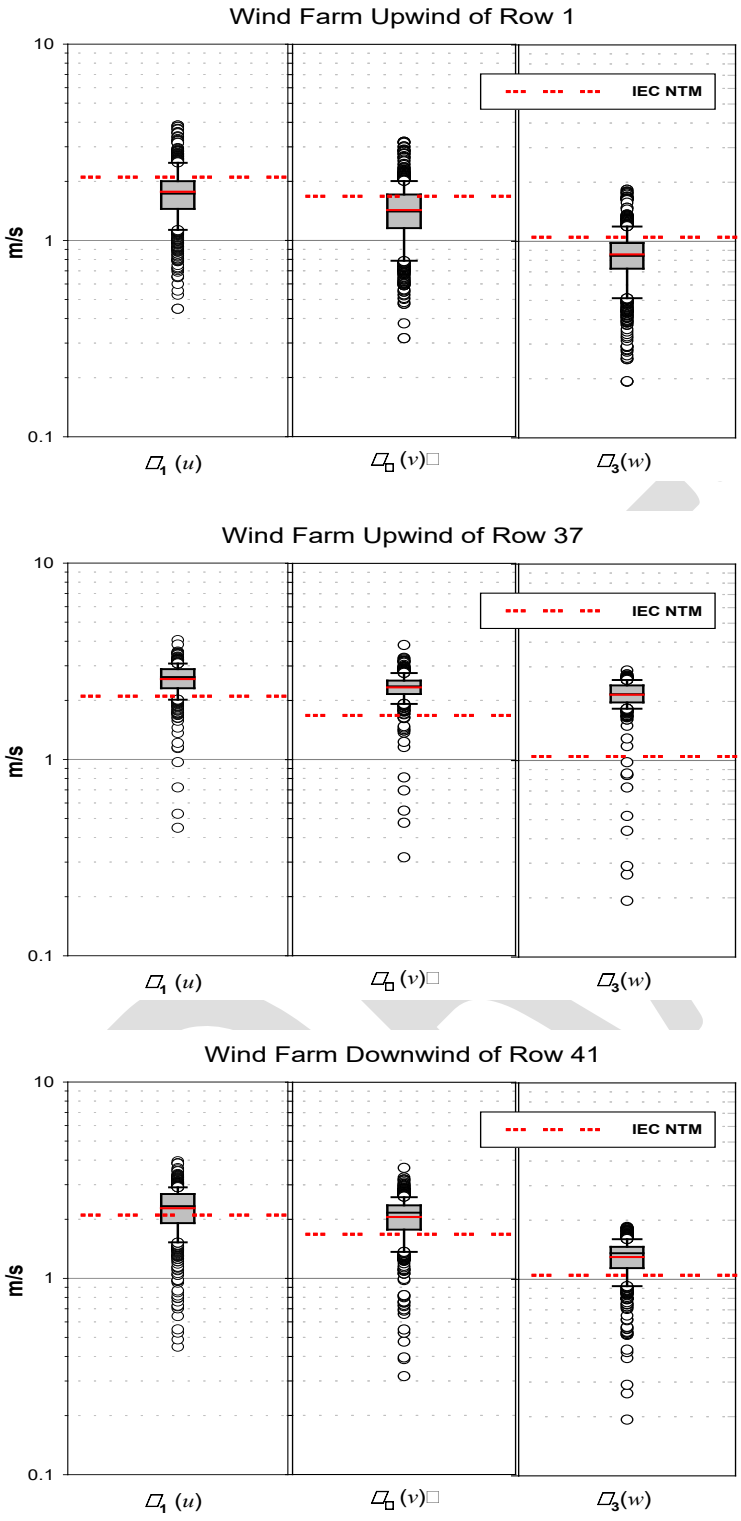

Figure 26a. Box plot distributions of the hub-height standard deviations of the streamwise, crosswind and vertical turbulent wind components measured at the three locations in the California wind farm. The corresponding values for the IEC Class 1 NTM are shown as the red dash-dot-dot lines

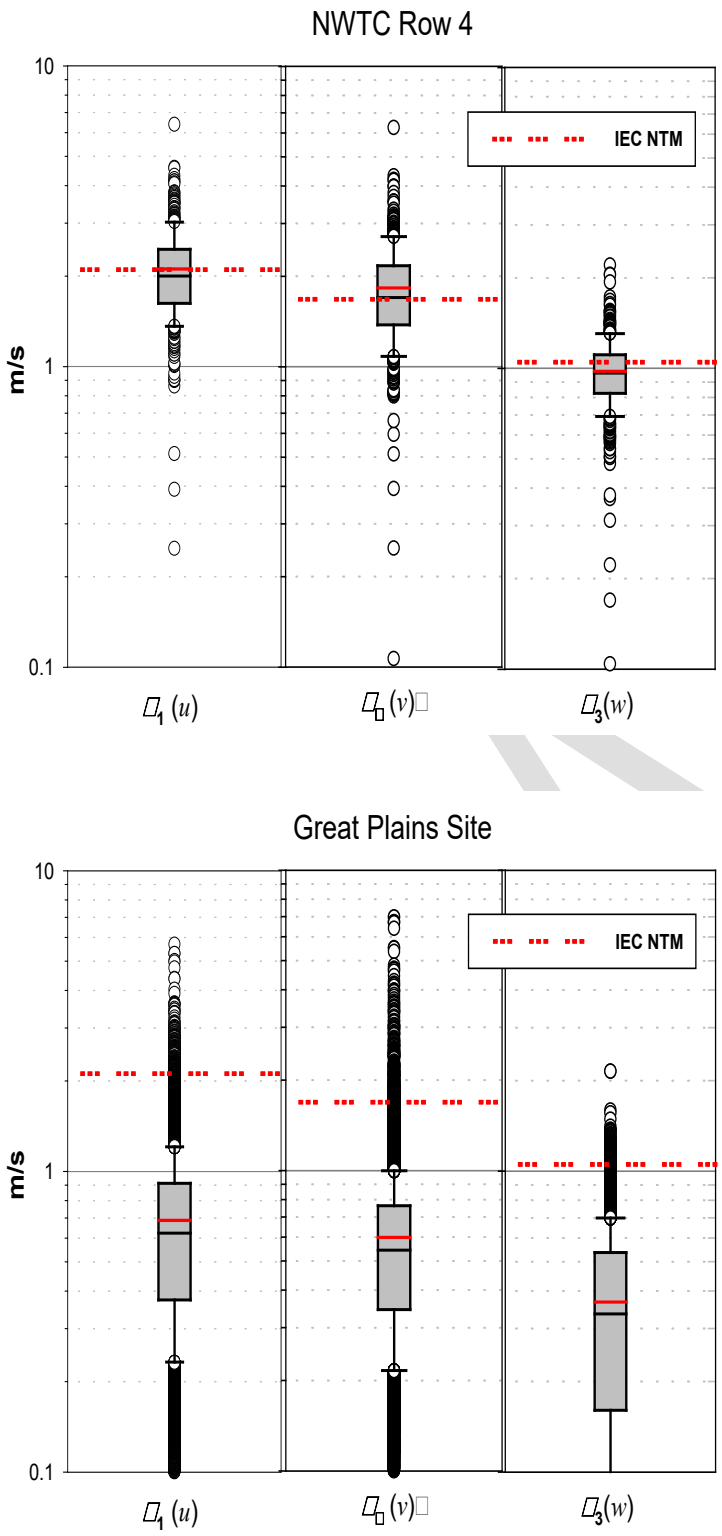

Figure 26b. Same as Figure 26a but for the NWTC Row 4 and the Great Plains Sites

Inherent in the flows entering the rotor disks at all three of these sites are the presence of coherent turbulent structures. While there were no corresponding turbine aeroelastic measurements available for the Great Plains Site, the great number and severity of events with high values of σ_1 and σ_2 (the streamwise and crosswind directions) shown in Figure 26b suggest intense peak turbine loads induced by coherent structures occurring commonly. Figure 27 plots the occurrence of peak values of the blade FBM from the NWTC ART and Micon 65 as a function of the Turbine Layer Ri_{TL} and the CTKE of the responsible coherent structures. The critical stability range CRR of Table 4 is indicated by the dashed lines.

A close inspection of these plots reveals that the largest (and most damaging) peaks occur within the CRR stability range with those from the Micon being the most distinct. This figure demonstrates the criticality of including coherent eddy structures in any inflow simulations used with simulations of small wind turbines. The analysis of the NWTC ART and the Micon turbines' structural response found that the threshold sensitivity of coherent intensity (CTKE), beyond which a *significant* aeroelastic response is induced, is 10 m^2/s^2. This is indicated in the plots of Figure 25.

3.2.9 Configuring the TurbSim Simulator for the Recommended S1 to S6 Load Cases

For a complete discussion of the uses of TurbSim, see Kelley and Jonkman 2007. The discussions that follow are based on Version 1.50 of TurbSim; the user's guide prepared by B.J. Jonkman is available online (Jonkman 2009). Both references and the code can be downloaded from the NWTC Information Portal https://nwtc.nrel.gov/TurbSim.

Communication with TurbSim occurs through the TurbSim Input File, an example of which is presented in Figure 28. TurbSim reads these specified parameters for the program to execute. *It assumes that parameters are located on specific lines of the input file*. None of the parameters are case sensitive. The parameters that deal with the definition of the simulation space and its time-dependent characteristics are not highlighted. Those that are important to these recommended load cases include the vertical and horizontal grid matrix dimensions (`NumGrid_Z` and `NumGrid_Y`), the time step (`TimeStep`). The grid definition parameters `GridHeight` and `GridWidth` along with the `HubHt` are dependent on the turbine being modeled.

The grid dimensions determine the spatial resolution of the simulated wind field. It is important that these dimensions are adequately small enough to allow for a reasonable representation of the important unsteady aerodynamic processes, such as dynamic stall, to take place when encountering a coherent structure. Ideally this dimension should be in the range of three to five blade chord widths or even smaller at 75% span. Modern desktop computers generally have more than enough resources to achieve such a minimum resolution and have sufficient computing power to complete a 630 s (over 10 minutes of real time data) solution in a reasonable amount of wall clock time. For example, for a modeled rotor of a small wind turbine in the horizontal-axis wind turbine configuration with a diameter of 20 m and a 75%-span chord width of 15 cm, a 44x44 grid matrix would meet these criteria. It is further recommended that each individual simulation (stochastic realization) of 630 s in length with a time step be 0.05 s to provide sufficient temporal resolution of important turbulent processes. To obtain a reasonable statistical sample for the boundary conditions defined by each of the six proposed Special Load

Classes (S1-S6), it is recommended that *at least 31* individual realizations (each using a new random seed) be calculated in order to apply large sample statistics to the ensemble of simulations.

Figure 28 highlights the parameters of the meteorological and non-IEC meteorological boundary conditions specified in the TurbSim Input File to apply the conditions for each of the recommended six Special Load Classes S1-S6. The values of these parameters are presented in Table 5. It is recommended that, at a minimum, 31 realizations of each of the six load cases defined in Table 5 be calculated and used as a suite of inflow conditions to an aeroelastic code such as FAST or a multi-body code such as ADAMS® or Simpack. The application of this suite of inflows will allow the designer to obtain a comprehensive look for potential high-fatigue damage areas in a new turbine (or existing) turbine configuration that can be verified by field measurements.

The choice of the hub-height mean wind speed of 10 m/s is an extension of the value used in the current IEC Class 1 standard. Choosing this velocity is supported by the observation that significant unsteady aerodynamically induced loading events occur during near-rated to slightly under-rated conditions. Table 6 summarizes the level of severity associated with each of the defined load cases in Table 5. Based on the contents of this table, it appears that Special Class 2 is likely to provide the most vigorous inflow turbulence environment in the proposed suite of simulations. While it does not have the greatest number and total length of coherent structures, the average intensity of those observed is greater than Special Class 3, which has more structures but less average intensity.

3.2.10 Considerations When Using the FAST/AeroDyn Aeroelastic Simulation Codes

A discussion of the use of the FAST/Aerodyn codes is beyond the scope of this section. The latest versions of FAST and AeroDyn are FAST v8 and AeroDyn v15, both of which support the latest code innovations. It is *strongly recommended* that when using the FLAP/AeroDyn simulators, the *Generalized Dynamic Wake* option is used in place of the Blade Element Momentum choice. The use of the Generalized Dynamic Wake option is necessary to obtain the most significant unsteady structural responses and resulting impulsive loads from coherent structures in the simulated inflow. These codes are being developed, and it is highly recommended that the user check with the NWTC regarding the availability and use of the Generalized Dynamic Wake option with FAST v8. The NWTC Design Codes Computer-Aided-Engineering software tools may be accessed through the link https://nwtc.nrel.gov/CAE-Tools.

DRAFT

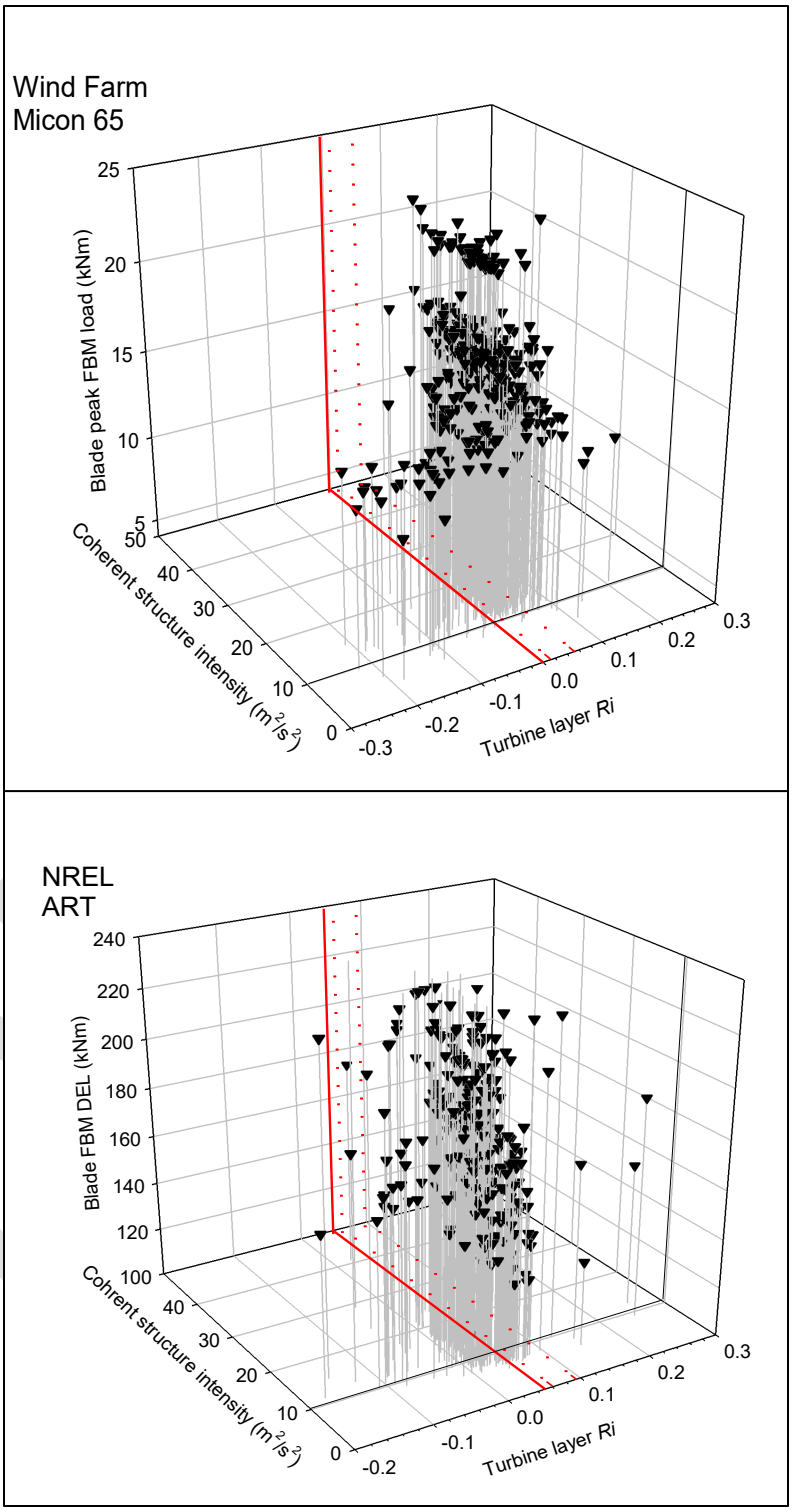

Figure 27. Peak FBM loads seen on the NWTC ART and Micon turbines as a function of the turbine layer Ri_{TL} and the intensity (CTKE) of the coherent structure responsible

Figure 28. Example of TurbSim Input File, which has been annotated to indicate the parameters that must be changed to accommodate the boundary conditions specified by the recommended Special Load Classes S1-S6

Table 5. TurbSim Input Parameters for Simulating Recommended Special Load Classes S1-S

@The CTEventfile parameter must provide the path containing the files of the coherent events; e.g., H:\coh_events\eventdata

	TurbModel	IECturbc	ProfileType	RefHt (m)	URef (m/s)	ZJetMax (m)	PLExp	RICH_NO	Ustar (m/s)	PC_UW	PC_UV	PC_VW	Coh Structures?@
Special Class S1	WF-UPW		PL	hub height	10		0.171	0.02	0.489	-0.241	-0.114	0.061	Yes
Special Class S2	WF-07D		PL	hub height	10		0.128	0.02	1.165	-1.407	-0.454	0.346	Yes
Special Class S3	WF-14D		PL	hub height	10		0.17	0.02	1.079	-1.189	0.085	-0.144	Yes
Special Class S4	NWTCUP		PL	hub height	10		0.156	0.02	0.633	-0.471	0.712	-0.341	Yes
Special Class S5	GP_LLJ		JET	hub height	10	200		0.02	0.419	-0.191	0.12	0.042	Yes
Special Class S6	NWTCUP	KHTEST		hub height	10				0.621	-0.377	0.321	-0.204	Yes

Table 6. Comparison of IEC Class 1 and Special Classes Wind Component Turbulence Levels and Coherent Structure Properties

					Average over 10-minutes Coherent Structure		
					Total	Intensity	Number of
	I_{15}	σ_1	σ_2	σ_3	Length	CTKE	structures
		(m/s)	(m/s)	(m/s)	(s)	(m^2/s^2)	in record
IEC Class 1	0.18	2.100	1.680	1.050	?	?	?
Special Class 1	0.12	1.769	1.428	0.859	26.2	10.9	14.6
Special Class 2	0.17	2.731	2.390	2.175	42.7	15.8	31.8
Special Class 3	0.18	2.625	2.302	2.159	67.8	14.5	38.5
Special Class 4	0.15	2.214	1.834	1.020	45.5	12.6	15.2
Special Class 5	0.09	1.119	0.793	0.519	57.3	14.8	17.9

3.3 Calculation of EDC Magnitude for Highly Turbulent Sites

Extreme direction change (EDC) is a rapid change in wind direction and is typically one of the design-driving loads cases, which includes potential effects of wind turbulence. When designing an urban/rooftop wind turbine or a turbine in a highly turbulent site, it is recommended that the formula of EDC be modified with a higher magnitude to capture increased turbulence effects currently found in IEC 61400-2 third edition.

The EDC currently shows magnitude for a recurrence period of *N* years given by:

$$\theta_{eN}(t) = \pm\beta \arctan\left(\frac{\sigma_1}{V_{hub}\left(1+0.1\left(D/\Lambda_1\right)\right)}\right). \quad (13)$$

Here, σ_1 is the standard deviation of the longitudinal wind velocity component, Λ_1 is the turbulence scale parameter, D is the rotor diameter, β is 4.8 for $N = 1$ year and 6.4 for $N = 50$ years.

For the NTM, the value of σ_1 is calculated by

$$\sigma_1 = \frac{I_{15}(15 + aV_{hub})}{a+1}. \quad (14)$$

Here, I_{15} is the TI at 15 m/s, a is a dimensionless slope parameter and V_{hub} is the longitudinal velocity at hub height. The values of I_{15} and a are 0.18 and 2, respectively, for all small wind turbine classes. However, for urban/rooftop installations, the values of I_{15} are generally higher than 0.18.

Figure 29 shows the results of a measurement campaign conducted from August 2011 to July 2012 on a rooftop of an 8-m Nasu-Denki Tekko Co. Ltd. building in Tokyo. By linearly extrapolating the measurement data above V_{hub} = 10 m/s to V_{hub} = 15 m/s, I_{15} of the measurement is estimated as $I_{15\_obs} \approx 0.3$.

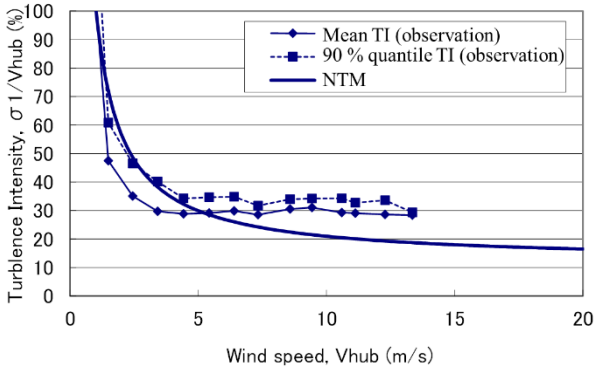

Figure 29. Turbulence intensity vs. wind speed at hub height

Figure 30 shows the EDC magnitude for a recurrence period of 1 year vs. wind speed at hub height. The measurement data were obtained in the above mentioned measurement campaign. The original IEC model for EDC magnitude (i.e., Equation 13 with $I_{15} = 0.18$) significantly underestimates the 90% quantile of the EDC magnitude. In the case of using $I_{15} = 0.3$ ($\approx I_{15\_obs}$), Equation 15 approaches the 90% quantile of the EDC magnitude obtained; however, it is still significantly underestimated.

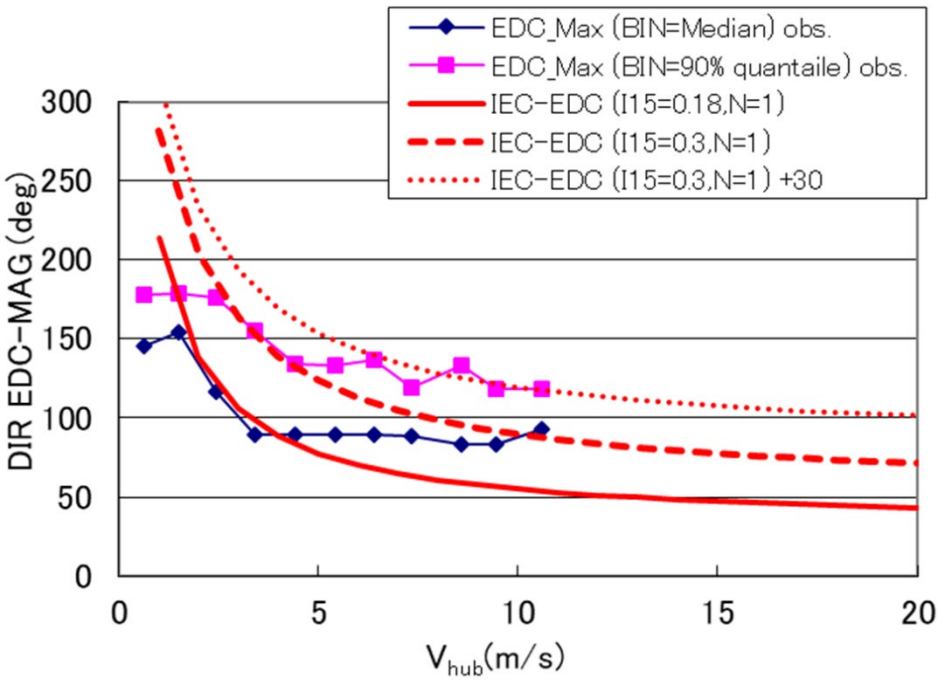

Figure 30. EDC magnitude vs. wind speed at hub height for Nasu-Denki measurement site

The addition of 30˚ to Equation 13 shows an $I_{15} = 0.3$, which is generally larger than the 90% quantile of the EDC magnitude measurements and also shows a reasonable match for the high-wind-speed range. Therefore, Equation 13 is modified below for a recurrence period of N years for urban/rooftop installations as follows:

$$\theta_{eN}(t) = \pm\beta \arctan\left(\frac{\sigma_1}{V_{hub}\left(1+0.1\left(D/\Lambda_1\right)\right)}\right) + 30° \quad . \qquad (15)$$

The value "30°" should be updated by accumulating more EDC observation data at many different sites.

3.4 VAWT Simplified Load Methodology

Simplified load methodology for a VAWT is proposed by the experts in Mie Univ. and the Japan Small Wind Turbines Association under the NEDO R&D Program (FY 2008~2012). This R&D activity intended to form the technical background for the Japanese feed-in tariff system, which started in 2012. The VAWT simplified loads methodology was a key issue since several commercial small VAWTs would need to meet standard requirements to be able to apply for the feed-in tariff.

This simplified load methodology was developed with the same logic as the simplified load methodology for the horizontal-axis wind turbine described in IEC 61400-2. Most simplified load equations were based on conventional mechanical engineering and fluid dynamics supported by wind tunnel testing.

In 2013, the R&D result was added into JSWTA0001 standard (Small Wind Turbine Performance and Safety Standard), which is a national industrial standard almost equivalent to IEC 61400-2. This simplified load methodology is written in Annex C (formative) of JSWTA0001 and titled "Development of the simple design equations for a vertical-axis wind turbine (VAWT)."

3.4.1 Main Features

The main features identified for the VAWT simplified loads methodology include the following:

- Applies to a vertical-axis rotor symmetry with respect to its equatorial plane
- Applies to a rotor with up to five blades (based on wind tunnel experiments conducted on VAWTs with up to five blades)
- A deflection limit based on MATLAB Simulink Simulations. The deflection of the rotor shaft is not larger than 0.3 % at its center under the load case H (found in JSWTA0001) and thereby such a cantilever structure system that the rotor shaft is supported at its first bearing and may be assumed to be dynamically stable
- No wind shear is considered.

Wind shear effect on fatigue does not need to be considered because the cyclic variation of blade angle of attack due to its rotation is much larger than that due to wind shear.

3.4.1.1 Load Case A: Normal Operation

(1) Loads on blade

For design rotor speed, the difference between the maximum force and the minimum force on a blade during one cycle (= maximum amplitude) is given by Equation 17, based on experimental result of force in the direction parallel to wind flow under various tip speed ratio.

$$\Delta F_{\mathrm{xB}} = \frac{1}{2}\rho A_{\mathrm{proj,B}}(1.5V_{\mathrm{design}})^2 \cdot \left(8.5\lambda_{\mathrm{design}} - 3.2\right) \quad (17)$$

ΔF_{xB} is the amplitude of the force acting on a blade in X_B direction (flap-wise direction and in the radial direction of the rotor)

$A_{\mathrm{proj,B}}$ is maximum projection area of a blade (area in plain view)

The numerical values in Equation 17 were determined from the highest value calculated for 7 airfoil sections NACA0008、0012、0016、0020、0024、0028、0032.

The thrust on the rotor shaft in operation is given as:

$$F_{\mathrm{T}} = C_{\mathrm{T}}\frac{1}{2}\rho(1.5V_{\mathrm{design}})^2 A \quad (18)$$

Thrust coefficient C_T = 1.2 was determined by wind tunnel tests for 2, 3, 4 and 5- bladed VAWTs (Figure 31).

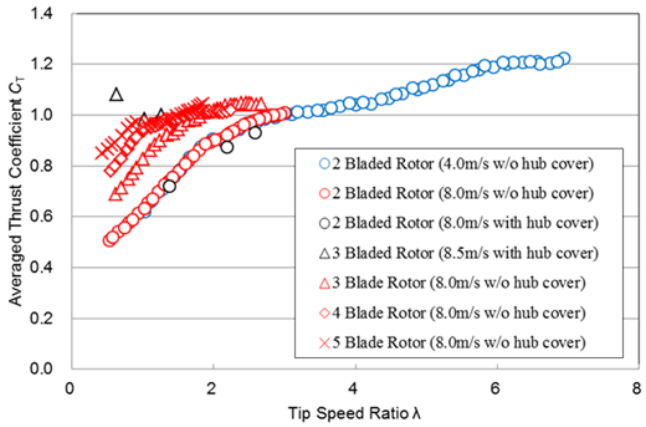

Figure 31. Wind tunnel test data: Averaged Thrust Coefficient vs. Tip Speed Ratio for 2, 3, 4 and 5-bladed VAWTs

3.4.1.2 Load Case H: Survival Wind, Loads on Rotor Shaft

The drag acting on the blades of a parked rotor generates wind force on the rotor shaft:

$$F_{\text{shaft}} = C_{\text{Fshaft}} \frac{1}{2} \rho A_{\text{proj,B}} V_{\text{e50}}{}^2 \quad (19)$$

The wind tunnel measurements of thrust coefficient C_{Fshaft} are given in Table 7, depending on the number of blades.

Table 7. Thrust Coefficient C_{Fshaft} Acting on a Parked Rotor

B	1	2	3	4	5
C_{Fshaft}	1.1	2.0	2.0	2.9	3.2

The values of thrust coefficient C_{Fshaft} were determined by wind tunnel tests for 2, 3, 4 and 5-bladed VAWTs.

4. KEY CONCLUSIONS/RECOMMENDATIONS

The above technical discussions have been initially validated by comparing several different data sets. Chapter 2 results were largely informed by the Belgian datasets for urban and peri-urban sites, by the Australian urban site data compared to data from a Swedish island, and by the urban site in Tokyo, Japan. For Chapter 3, the vibration discussion was developed by urban test site results from Austria. The assessment of small wind turbine structural component fatigue damage is based on Neil Kelley's extensive turbulence measurement, analysis and code development experience and used three data sets to highlight fatigue and DEL sensitivities during weakly stable conditions around turbine rated power. Finally, the recommendations for changing EDC and introducing a simple load model for a VAWT design are based on Tokyo urban test results and the VAWT simplified load methods developed by Japanese colleagues, respectively.

In the course of conducting research and developing this technical report, the authors are aware that this is a "stepping-stone" on the way to a normative standard. As is natural in such a case, a few areas have been identified in which stakeholders would benefit from further research and validation on the recommendations given in this report.

- TI is strongly site dependent and for a given site may depend on the wind direction. We recommend that the technical experts involved in a small wind turbine project be aware of this fact and take into account the sensitivities in wind direction as part of their site assessment.
- For highly turbulent sites, the NTM of the IEC 61400-2 standard underestimates the level of turbulence and uses a reference wind speed for which data are likely to be sparse. We therefore recommend two values to be used as a reference wind speed, in accordance with the definition of a new turbulence model more suited to highly turbulent sites presented in Equation (3): 5 m/s for a low-speed regime up to 6.5 m/s and 10 m/s for the high-speed regime. This way an individual with no measurements or assessment of turbulent wind conditions for a turbine site could use the new NTM to more appropriately model the design conditions and, with it, the fatigue loads. For later analysis, of particular importance would be the reference wind speed in the high-wind regime (10 m/s), where most of the destructive transient aerodynamic rotor loads occur. Whenever known, the turbine-rated wind speed should be used instead to appropriately scale the TI value.
- More data are needed to validate the addition of 30 degrees to the modified EDC equation, which was based on measurements for a low-rise rooftop. Adding a variety of measurement sites would improve the robustness of this modified equation.
- To better capture the wind conditions found in highly turbulent sites, a new design classification (Tu, urban or highly turbulent) presented in Table 2 should be considered for all small wind turbines installed in urban and peri-urban sites (or generally speaking, high-turbulence sites).
- Small wind turbine tower systems should be designed in a way that guarantees an overcritical mode of operation within the range of 70% PN to full rated power when stimulating forces are relatively high.
- Small wind turbine tower systems should be designed to have as high a structural damping factor as possible. Damping factors between 10% and 20% are desirable. To increase the structural damping and reduce natural frequencies, damping or decoupling elements may be used.
- Resonances are likely to occur within the tower-rotor system as the natural frequency of these structures often fall in the critical frequency range matched at high wind speeds by the rotor. If these resonances can't be mitigated to a non-critical operation range, critical RPM ranges shall be avoided by means of turbine RPM control.
- For VAWWT simplified loads methodology, advising caution as wind shear, depending on the size of the turbine, might add to DEL already coming from cyclic variations of rotor blade attack angles. This might not have an immediate impact but, over time, with accumulation of fatigue damage, the wear and tear of a machine is likely to increase at a faster rate if wind shear is accounted for. In addition to that, some VAWT designs aim for

individual blade pitch control, taking into account the azimuthal locations of the blade. In this situation, that blade loads are controlled and diminished, thus wind shear and coherent structures will be of greater importance.

- If practically feasible, the quality of the site assessment and load prediction can be greatly improved by the following approach:
    - Measure temperature at two heights and use these to derive the Richardson number. Weakly stable conditions in the range $0.01 \leq Ri < 0.05$ are expected to lead to increased fatigue damage.
    - Use three-dimensional ultrasonic anemometers to assess the friction velocity and/or shear stress. Large values of the friction velocity, in combination with weakly stable conditions defined above, are expected to lead to increased fatigue damage.
    - Site evaluations for new turbine installations should include not only wind resource characterization in terms of the annual 10-minute mean wind speed distribution but also, if possible, number of hours of expected operation at rated wind speed within the critical stability range. As a proxy for the stability requirement, it may be considered to stratify the 10-minute mean wind speed statistics diurnally (i.e., into 24-hour records). Of importance then are the expected annual number of hours in which the small wind turbine will be operating at near rated wind speed ($V_{rated} \sim \pm 10\%$) and within the critical stability range.

Further work is needed to validate these initial results and verify the proposed recommendations for changes in IEC 61400-2. Details for field data collection to support model validation are given in Appendix A.

REFERENCES

Arany, L., Bhattacharya, S., Macdonald, J., and Hoga, S.J. 2014. *Simplified critical mudline bending moment spectra of offshore wind turbine support structures.* Wind Energy online. https://www.researchgate.net/publication/267517615_2014_Wind_Energy_online.

Arya, S.P. 2001. *Introduction to micrometeorology.* AP International Geophysics Series.

Balduzzi F., Bianchini SA., Ferrari L. Microeolic turbines in the built environment: Influence of the installation site on the potential energy yield. Renewable Energy 2012, 45: 163-174.Burton, T., Jenkins, N., Sharpe, D., Bossanyi, E., 2001. *Wind Energy Handbook*. John Wiley & Sons, Ltd: Chichester, West Sussex.

BAUA. 2016. Vibrationen. //www.baua.de/de/Themen-von-AZ/Vibration/Vibration_content.html. Accessed 21.04.2016.

Byrne, R., Hewitt, N. J., Griffiths, P., and MacArtain, P. 2018. *Observed site obstacle impacts on the energy performance of a large scale urban wind turbine using an electrical energy rose.* Energy for Sustainable Development, 43, pp. 23 - 37. DOI: 10.1016/j.esd.2017.12.002.

Evans S., Anup KC, Bradney D., Urmee T., Whale J., Clausen P. The suitability of the IEC 61400-2 wind model for small wind turbines operating in the built environment. Renew. Energy Environ. Sustain. 2, 31 (2017).

Hansen, M.O.L. 2008. *Aerodynamics of wind turbines*. 2nd ed, Earthscan from Routledge.

Jonkman, B.J. 2009. *TurbSim User's Guide: Version 1.50,* NREL/TP-500-46198, Golden, CO: National Renewable Energy Laboratory, https://www.nrel.gov/docs/fy09osti/46198.pdf.

Kelley, N.D. 2011. *Turbulence-Turbine Interaction: The Basis for the Development of the TurbSim Stochastic Simulator*, NREL/TP-5000-52353, http://www.nrel.gov/docs/fy12osti/52353.pdf.

Kelley, N. D. and Jonkman, B.J. 2007. *Overview of the TurbSim Stochastic Inflow Turbulence Simulator: Version 1.21* NREL/TP-500-41137, Golden, CO: National Renewable Energy Laboratory. https://www.nrel.gov/docs/fy07osti/41137.pdf.

N.D. Kelley, B.J. Jonkman, G.N. Scott, J.T. Bialasiewicz, L.S. Redmond. 2005. *The Impact of Coherent Turbulence on Wind Turbine Aeroelastic Response and Its Simulation*. NREL/CP-500-38074. https://www.nrel.gov/docs/fy05osti/38074.pdf.

Kuttner. 2015. Praxiswissen Schwingungsmesstechnik, Springer Vieweg, Wiesbaden. VDI Wissensforum GmbH, 6. VDI-Fachtagung Schwingungen von Windenergieanlagen 2015, 2015, Bremen, VDI-Verlag Dusseldorf, ISBN 978-3-18-092242-3.

Magnus, Popp, Sextro. 2008. Schwingungen – Eine Einfuhrung in die physikalischen Grundlagen und die theoretische Behandlung von Schwingungsproblemen, 8. Auflage, Vieweg + Teubner Verlag, Wiesbaden.

Peppoloni, M., Hirschl, A., Leonhartsberger, K. 2017. Environmental Influences on SWT - Vibrations and Oscillations, proceedings of the 2017 TUrbWind Colloquium, Riva del Garda, Italy.

Petersen, E.L., Mortensen, N.G., Landberg, L., Hujstrup, J., Frank, H.P. 1998. *Wind Power Meteorology. Part I: Climate and Energy*, Wind Energy 45, 25.

Rafailidis s. Influence of building areal density and roof shape on the wind characteristics above a town. Boundary-Layer Meteorology, 1997,8592:255-271.

St. Martin, C.; Lundquist J., Clifton A., Poulos G., and Schreck S. Wind turbine power production and annual energy production depend on atmospheric stability and turbulence. European Academy of Wind Energy, 2016, Wind Energy. Sci.1, 221-236

Stull, R.B. 2012. *An introduction to boundary layer meteorology* (Vol. 13). Springer Science & Business Media.

Tabrizi, A., Whale J, Thomas L, et al. Performance and safety of roof top wind turbines: Use of CFD to gain insight into inflow conditions. Renewable Energy, 2014, 67(7): 242-251.

Taylor, G.I. 1938. *The Spectrum of Turbulence*. Proceedings of the Royal Society A: Mathematical, Physical and Engineering Sciences. 164: 476–490.

Toja-Silva F., Peralta ., Lopez-Garcia, O.. Roof region dependent wind potential assessment with different RANS turbulence models. Journal of Wind Engineering and Industrial Aerodynamics 2015; 142: 258-271.

Toja-Silva F., Kono T., Peralta C., Lopez-Garcia O., Chen J. *Journal of Wind Engineering & Industrial Aerodynamics*. 180 (2018) 66–87.

Twele. 2013. Empfehlungen zum Einsatz kleiner Windenergieanlagen im urbanen Raum – Ein Leitfaden, HTW Berlin, Berlin.

Veers, P.S. 1988. Three-dimensional wind simulation, Tech. report, Sandia National Laboratories.

Wang B., Cot L. D., Adolphe L., et al. Estimation of wind energy over roof of two perpendicular buildings [J]. Energy and Buildings, 2015, 88(2): 57–67.

Wang Q., Wang J., Hou Y., et al. *Micrositing of roof mounting wind turbine in urban environment: CFD simulations and lidar measurements*. Renewable Energy, 2018, 115:1118-1133.

Appendix A. Details for Designing a Field Measurement Campaign

It is strongly suggested that small wind turbine designers utilize the simulation modeling approach discussed in (5.2) in conjunction with loads measurements for validation purposes. Application of an aeroelastic code such as FAST configured with the aerodynamic, mechanical and material properties of the design turbine and validated with field measurements should be used as the basis to accomplish the requirement elements of the certification process.

To obtain the most useful field measurements, it is recommended that load measurements be made at a test site that has flat, uniform terrain upstream in the dominant power wind direction(s). To obtain the most information in the minimum amount of field time, it is recommended that the load and turbine dynamics measurements be performed for a period of at least 30 hours of 10-minute records with a hub mean wind speed equal to the turbine rated speed ± 2 m/s and residing within a Ri_B stability range of +0.01 to +0.05. It is within these ranges that the largest loads and extremes can be expected. This data set should be used for the subsequent safety analyses. Figure A-1 is a schematic of the minimal field instrumentation arrangement for obtaining a measure of the Ri_B; Equation A-1 is needed to establish the above criteria. A useful addition to this basic configuration would be to add a three-dimensional sonic anemometer at hub height that is capable of making and recording the u_1, u_2 and u_3 component wind velocities at a rate of at least 10 Hz but preferably at 20 Hz. An accompanying value of the shear velocity u_* is also needed. Ideally that would be measured by a hub-height sonic anemometer from $\overline{u_1' u_3'}$ but can be estimated by the following equation using the wind speeds from the two heights.

$$u_* = 0.4(\overline{U_2} - \overline{U_1}) / \ln(z_2 / z_1) \qquad \text{(A-1)}$$

These data can also be used to validate simulation modeling of the small wind turbine design for the observed operating conditions and to anticipate the turbine response over a range of operating conditions using the turbulence spectral models available in the NREL TurbSim Stochastic Simulator. However, the best approach is to use a sonic anemometer to obtain measured values of the mean Reynolds stresses, $\overline{u_1' u_3'}, \overline{u_1' u_2'}, \& \overline{u_2' u_3'}$, that can then be used for scaling for the TurbSim input variables `PC_UW`, `PC_UV`, and `PC_VW`.

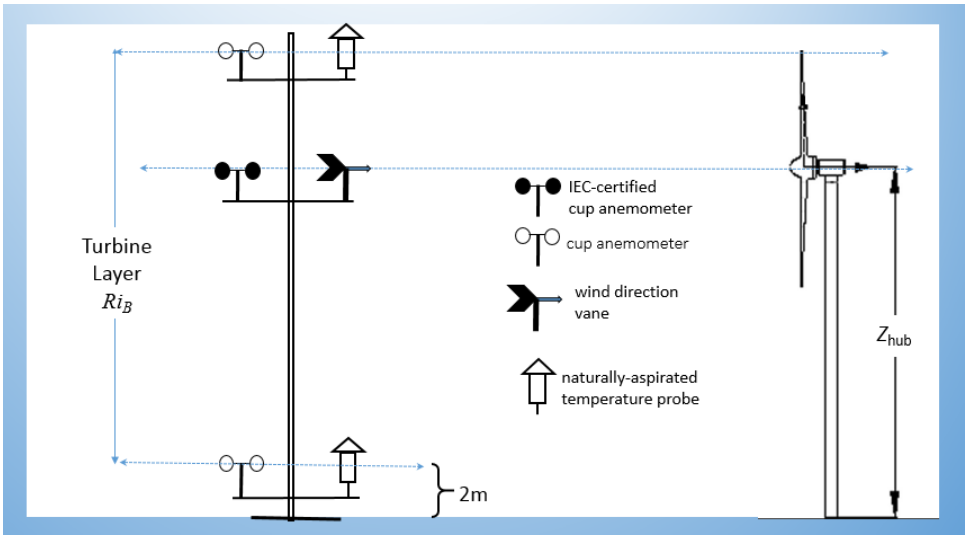

Figure A-1. Schematic of a basic instrumentation configuration to obtain wind inflow and stability information for obtaining load measurements within the critical range of +0.01 ≤ Ri < +0.05